Atmospheric
Chemistry
and Physics

Yields and molecular composition of gas-phase and secondary organic aerosol from the photooxidation of the volatile consumer product benzyl alcohol: formation of highly oxygenated and hydroxy nitro-aromatic compounds

Mohammed Jaoui[1], Kenneth S. Docherty[2], Michael Lewandowski[1], and Tadeusz E. Kleindienst[1]

[1]Center for Environmental Measurement & Modeling, U.S. Environmental Protection Agency,
Research Triangle Park, NC 27711, USA
[2]Jacobs Technology, Inc., Research Triangle Park, NC 27709, USA

Correspondence: Mohammed Jaoui (jaoui.mohammed@epa.gov)

Abstract. Recently, volatile chemical products (VCPs) have been increasingly recognized as important precursors for secondary organic aerosol (SOA) and ozone in urban areas. However, their atmospheric chemistry, physical transformation, and impact on climate, environment, and human health remain poorly understood. Here, the yields and chemical composition at the molecular level of gas- and particle-phase products originating from the photooxidation of one of these VCPs, benzyl alcohol (BnOH), are reported. The SOA was generated in the presence of seed aerosol from nebulized ammonium sulfate solution in a $14.5\,\mathrm{m^3}$ smog chamber operated in flow mode. More than 50 organic compounds containing nitrogen and/or up to seven oxygen atoms were identified by mass spectrometry. While a detailed non-targeted analysis has been made, our primary focus has been to examine highly oxygenated and nitro-aromatic compounds. The major components include ring-opening products with a high oxygen-to-carbon ratio (e.g., malic acid, tartaric acids, arabic acid, trihydroxy-oxo-pentanoic acids, and pentaric acid) and ring-retaining products (e.g., benzaldehyde, benzoic acid, catechol, 3-nitrobenzyl alcohol, 4-nitrocatechol, 2-hydroxy-5-nitrobenzyl alcohol, 2-nitrophloroglucinol, 3,4-dihydroxy-5-nitrobenzyl alcohol). The presence of some of these products in the gas and particle phases simultaneously provides evidence of their gas–particle partitioning. These oxygenated oxidation products made dominant contributions to the SOA particle composition in both low- and high-NO_x systems. Yields, organic mass to organic carbon ratio, and proposed reaction schemes for selected compounds are provided. The aerosol yield was 5.2 % for $BnOH/H_2O_2$ at an SOA concentration of $52.9\,\mathrm{\mu g\,m^{-3}}$ and ranged between 1.7 % and 8.1 % for $BnOH/NO_x$ at an SOA concentration of $40.0\text{–}119.5\,\mathrm{\mu g\,m^{-3}}$.

1 Introduction

Modeling atmospheric organic aerosol (OA) using chemical transport models (CTMs) is complex, challenging, and often leads to model–measurement discrepancies (Zhao et al., 2016). Applying CTMs to urban areas reveals that traditional volatile organic compounds (VOCs) including combustion-related processes cannot account for the observed OA mass, leaving a substantial fraction unresolved (Hayes et al., 2015). Recent studies suggest that this discrepancy is due in part to unaccounted for, rapidly reacting SOA and ozone precursors from unknown sources (Hodzic et al., 2009; Hayes et al., 2015; McDonald et al., 2018; Akherati et al., 2019; Lu et al., 2020). Volatile chemical products (VCPs), such as per-

sonal care products, cleaning agents, coatings, adhesives, and pesticides, have emerged as possible sources in urban areas (McDonald et al., 2018). Their emissions can be larger than those from usual sources, such as motor vehicles (Coggon et al., 2021). Laboratory, modeling, and field studies for VCPs have been conducted to assess their potential to affect ambient OA and ozone formation in urban and suburban locations (McDonald et al., 2018; Khare and Gentner, 2018; Stockwell et al., 2021; Seltzer et al., 2021; Gkatzelis et al., 2021; Milani et al., 2021; Pennington et al., 2021; Coggon et al., 2021). The contribution of VCPs to ambient OA is not fully understood and only limited modeling studies have been reported (Mohr et al., 2015; Vlachou et al., 2018; Pennington et al., 2021; Qin et al., 2021; Seltzer et al., 2021). Additionally, few experimental and chamber studies of VCPs have been conducted with limited characterization of aerosol products (Wu and Johnston, 2016, 2017; Harrison and Wells, 2012; Charan et al., 2020, 2022; Humes et al., 2022). For example, the analysis of SOA from the oxidation of cyclic methyl siloxanes (Wu and Johnston, 2016, 2017; Fu et al. 2020; Alton and Browne, 2020; Charan et al., 2022) and cyclic siloxanes (Janechek et al., 2019) has been conducted. Kinetic studies with limited product characterization have been reported for the oxidation of benzyl alcohol (BnOH) by hydroxyl radicals (Bernard et al., 2013; Wang, 2015; Harrison and Wells, 2009, 2012). Recently, Humes et al. (2022) highlighted the importance of oxygenated aromatic VCPs emission to generate urban SOA and oxygenated products in both gas and aerosol phases. Therefore, understanding the atmospheric chemistry of VCPs is important to assess their role in air quality and climate and to improve SOA chemistry in CTMs, thereby allowing for better estimates in health studies and source apportionment.

The challenges associated with evaluating VCP impacts on urban OA can be addressed by identifying atmospheric VCP concentrations and SOA markers linking those VCPs to ambient particulate matter (PM). Benzyl alcohol (C_7H_8O) is an important ring-containing VCP used as an organic intermediate and a solvent in a wide range of applications (Antonelli et al., 2002). BnOH is also emitted from flowers and flowering trees (Do et al., 1969; Horvat et al., 1990; Larsen and Poll, 1990; Humpf and Scheier, 1991; Boatright et al., 2004; Vallat and Dorn, 2005; Orlova et al., 2006) and found in indoor air (Weschler, 2011). Gas kinetic studies of loss rates and product distributions have been conducted using flow tubes and environmental chambers. Bernard et al. (2013) examined the rate and mechanisms of the OH+BnOH reaction. Similarly, Harrison and Wells (2009, 2012) investigated the rate constants for the BnOH reaction with ozone, OH, and NO_3 radicals. Carter et al. (2005) conducted chamber experiments to assess ozone and PM formation from BnOH and related compounds. Product studies from BnOH oxidation have focused mainly on gas-phase (GP) products. Several carbonyl products, including benzaldehyde (BnAld), formaldehyde, glyoxal, butenedial, 4-oxopentanal, 3-hydroxy-2-propanaldehyde, benzyl nitrate, *o*-hydroxybenzyl alcohol, and *o*-dihydroxy benzene, were reported from the above studies. With respect to the particle phase (PP), Charan et al. (2020) reported aerosol yields from BnOH oxidation together with a limited number of SOA products. Finally, Wang (2015) conducted a theoretical study to elucidate the reaction mechanism of the oxidation of BnOH with OH radicals.

In this study, we report a detailed non-targeted chemical analysis of GP and SOA products originating from the photooxidation of BnOH in the presence and absence of oxides of nitrogen (NO_x), with the aim to better understand the chemical composition at the molecular level. Gas chromatography–mass spectrometry (GC-MS) and high-performance liquid chromatography were used for the identification of a range of organic compounds including oxygenated nitro-aromatics and related compounds bearing up to seven oxygen atoms. Nitro-aromatics are pollutants of concern due to their toxicity, light absorption properties, and relatively long residence times in the environment. Highly oxygenated compounds can partition into pre-existing particles or be involved in new particle formation. Also, in the present study, SOA and secondary organic carbon (SOC) yields were measured with the results compared to published data. A chemical mechanism is then proposed to represent and account for selected gas- and aerosol-phase products observed in this study.

2 Experimental methods

All chemicals including N, *O-bis*(trimethylsilyl) trifluoroacetamide (BSTFA) derivatization reagent with 1 % trimethylchlorosilane (TMCS) as a catalyst and benzyl alcohol (99 %), 2-methyl-4-nitrophenol, *L*-(+)-tartaric acid, *D*-(−)-tartaric acid, and meso-tartaric acid were purchased from Aldrich Chemical Co. (Milwaukee, WI) at the highest purity (99.8 %) available and were used without further purification. In addition to standards reported in our previous studies (Jaoui et al., 2004, 2018), 3-nitrobenzyl alcohol, benzoic acid, and 4-nitrocatechol were purchased from Tokyo Chemical Industry (OR, USA), while pentaric acid, 2,3-dihydroxy-4-methoxy-4-oxobutanoic acid, and arabic acid were obtained from Aurum Pharmatech, LLC (NJ, USA).

2.1 Chamber description and operation

All experiments were conducted in a 14.5 m³ fixed-volume chamber with TFE Teflon-coated walls and were maintained at a positive pressure of 0.1 Torr. The chamber operation, procedures, and instrumentation have been described previously (Kleindienst et al., 2006, 2009), and here just experiment-specific details are primarily included. A combination of fluorescent bulbs having radiation from 300–400 nm was used to photolyze NO_2. In the absence of NO_x, the radiation system was altered to include UV-313 sunlamps to adequately

photolyze H_2O_2. The chamber was operated in steady-state (SS or flow) mode to provide continuously stable effluent concentrations. Under these conditions, reactants and products equilibrate with the chamber surfaces to minimize irreversible losses of gases and particles. The SS operation allows for extended sampling periods to improve the accuracy and precision of the measurements (Shilling et al., 2008). Temperature, relative humidity, and UV light intensity were measured continuously with an uncertainty of 5 %. Pre-experiment and post-experiment procedures (see Sect. 2.5 below) were routinely carried out before and after each experiment to minimize contamination in the chamber. The reactant generation system provided constant sources of zero air, reactants, water vapor, and ammonium sulfate (AS) seed aerosol. The reactant flow of gases (e.g., NO_x) into the chamber was regulated using mass flow controllers. BnOH was injected using a syringe pump, vaporized in a heated glass bulb, and injected with zero air. For experiments in the absence of NO_x, a 50 % aqueous solution of H_2O_2 was vaporized, injected using a second syringe pump, and photolyzed to produce OH radicals. Typical chamber AS concentrations were approximately $1 \mu g m^{-3}$. Each SS experiment went through an initial transient period of 18–24 h until the reactant and product concentrations reached steady state.

2.2 Gas-phase measurements

A wide variety of instruments were used to measure the reactants and products. Nitric oxide (NO) and NO_x were measured with a TECO (Franklin, MA) oxides-of-nitrogen analyzer with an upstream nylon filter to remove nitric acid produced from $OH + NO_2$. The NO_x analyzer was calibrated with a NIST-traceable NO standard. Initial H_2O_2 concentrations were estimated by UV absorption using the ratio of the H_2O_2 to O_3 absorbances at 254 nm, as described by Kleindienst et al. (2009). Experiments in the absence of NO_x were conducted dry to avoid aqueous loss of H_2O_2. BnOH concentrations in the inlet and within the chamber were measured semi-continuously using an SRI model 8610C compact gas chromatograph with flame ionization detector (GC-FID; SRI Instruments, Torrance, CA). The purity of the BnOH was verified with GC-MS analysis.

Low-molecular-weight carbonyls and dicarbonyls were quantified by derivatization using 2,4-dinitrophenylhydrazine (Smith et al., 1989). Samples were collected at $0.5 L min^{-1}$ for 25 min and derivatized in a 4 mL solution of acidified DNPH and then heated for 40 min at 70 °C. Air samples were drawn for 20 min at a rate of $0.50 L min^{-1}$ through an impinger containing 5 mL of a DNPH solution in acetonitrile. The resulting solutions were analyzed by high-performance liquid chromatography with an ultraviolet detector (HPLC/UV) (Smith et al., 1989). A 15-component hydrazone standard (comprising formaldehyde-, acetaldehyde-, acrolein-, acetone-, propionaldehyde-, crotonaldehyde-,

methacrolein-, butyraldehyde-, 2-butanone-, BnAld-, glyoxal-, valeraldehyde-, m-tolualdehyde-, methylglyoxal-, and hexaldehyde; AccuStandard, Inc.) at a free carbonyl concentration of $30 \mu g mL^{-1}$ for each component was used for calibration. Separate dihydrazone standards of glyoxal-DNPH and methylglyoxal-DNPH were also formulated. Carbonyls were separated using a Hewlett-Packard (HP) 1100 HPLC system with an Agilent Zorbax ODS $4.6 \times 250 mm$, $5 \mu m$ column maintained at 30 °C eluted with binary acetonitrile–water gradient. A 10 μL injection volume was used for all standards and samples. Carbonyls were quantified by UV absorption with a diode array detector set to 360 nm. Control and sample processing were managed with HP ChemStation software. More highly oxidized gas-phase organic species were also collected with a 60 cm, four-channel XAD4-coated annular denuder for offline analysis (Jaoui and Kamens, 2001). Once collected, the denuders were extracted and analyzed according to the methodology described in Sect. 2.4 below.

2.3 Aerosol phase: bulk parameter measurements

Organic carbon (OC) was measured using a semi-continuous elemental carbon–organic carbon (EC-OC) instrument (Sunset Laboratories, Tigard, OR) (Offenberg et al., 2007). The pumping system draws chamber effluent through a quartz filter at a rate of $8 L min^{-1}$ with carbon-strip denuder to remove gas-phase organics that might interfere with the measurement. With a sample collection time of 0.5 h and an analysis time of 0.25 h, the duty cycle for the measurement of OC was 0.75 h (Lewandowski et al., 2015). The aerosol volume, size distribution, and total number density were measured using a scanning mobility particle sizer (SMPS), (model 3071A, TSI, Inc., Shoreview, MN) and a condensation particle counter (CPC) (model 3010, TSI, Inc., Shoreview, MN). The SMPS operating conditions were as follows: sample flow $0.2 L min^{-1}$, sheath flow $2 L min^{-1}$, and size scan from 19 to 982 nm.

2.4 Molecular characterization of GP and PP oxygenated organic products

A non-targeted chemical analysis was conducted focusing mainly on species bearing hydroxy and carboxylic groups (Jaoui et al., 2004, 2013, 2018). For each experiment, six 47 mm glass-fiber (GF) filters were taken for 24 h at a flow rate of $16.7 L min^{-1}$. A second set of samples used an in-line 60 cm XAD-4-coated annular denuder (followed by a GF filter) and was analyzed for gas-phase organic products (Jaoui and Kamens, 2001). After collection, GF filters were extracted by sonication with 5 mL methanol for 1 h, and denuders were extracted with 30 mL 1 : 1 dichloromethane / methanol mixture (Jaoui and Kamens, 2001). Prior to extraction, denuders and GF filters were spiked with *cis*-ketopinic acid (KPA), *trans*-*p*-menth-

6-ene-2,8-diol (PMD), and d_{50}-tetracosane (TCS) as internal and/or recovery standards (IS/RS). Denuder extraction solvents were rotary-evaporated to ~ 1 mL and filtered using 0.45 µm PTFE syringe filters. A 2 µL portion of this extract was analyzed by GC-MS (Jaoui and Kamens, 2001). The remaining denuder and filter extracts were evaporated to dryness under a gentle stream of N_2 at room temperature using an N-Evap evaporation bath (Organomation Associates, Inc., Berlin, MA), then derivatized with BSTFA (Jaoui et al., 2004). This technique provides a sensitive method for measuring low levels of highly oxidized organic compounds, including semivolatile and intermediate-volatility compounds in the GP and PP.

The GC-MS analysis was conducted on an Agilent GC (7890B) coupled with a quadrupole mass spectrometer (5977B). The injector, heated to 270 °C, was operated in splitless mode. Compounds were separated on a 60 m long, 0.25 mm i.d. RTx-5MS column (Restek, Inc., Bellefonte, PA) with a 0.25 µm film thickness. The GC oven temperature was initiated at 84 °C, held for 1 min, and then increased at 8 °C min^{-1} to 200 °C, followed by a 2 min hold, then an increase at 10 °C min^{-1} to 300 °C and a 15 min hold. The ion source, ion trap, and interface temperatures were 200, 200, and 300 °C, respectively. Mass spectra were collected in both the methane chemical (CI) and electron ionization (EI) modes.

2.5 Experimental and quality control procedures

Before each experiment started, the chamber was flushed with zero air (hydrocarbon-free) for 24 h from an Aadco clean generator (Cleves, OH, USA). Experiments were conducted in either the absence or presence of NO_x. For experiments with NO_x, BnOH and NO were added to the chamber through flow controllers to the target concentration. For experiments in the absence of NO_x, the photolysis of H_2O_2 was the source of OH. H_2O_2 as a 50 % aqueous solution was injected through a syringe pump into a heated glass bulb where it vaporized and was then mixed rapidly by the main dilution airflow. For these experiments, BnOH was added as described above. Ammonium sulfate seed aerosol was also introduced into the chamber for all experiments to serve as a condensing medium for semivolatile organic products that might form. After the reactants reached steady-state concentrations (24 h), the background was characterized using all instruments to check for artifacts including background GP and PP species. Background chamber air was also characterized using offline analysis of denuder and/or filters as described above. Previous studies show that BnAld and to a lesser extent benzoic acid, benzyl benzoate, and dibenzyl ether present either as impurity or as decomposition products upon BnOH exposure to air at room temperature or sonication (Urakami et al., 2000; Ferri et al., 2006; Abend et al., 2004). Here we investigated the effect of chamber air, sonication, and BSTFA derivatization on BnOH arti-

facts as described in the Supplement (Sect. S1). A small amount of BnAld impurity was detected using the direct injection (DI) method and estimated to be < 0.1 % in the purchased solution. When BnOH was exposed to clean air in the chamber in the absence of light, sonication, and/or BSTFA derivatization, our results show an additional low level of BnOH conversion to BnAld and benzoic acid using DI and BSTFA methods, which is similar to the findings of Abend et al. (2004), Urakami et al. (2000), and Ferri et al. (2006). Additional results and descriptions are provided in Sect. S1.

Experiments were initiated by turning on the lights and allowing the irradiated chamber effluent to reach SS conditions over a 24 h period, which permits active sampling by the online instruments and the collection of denuder and filter samples for subsequent offline analysis. For organic intermediates wall losses are typically not an issue due to reactions being conducted within a Teflon chamber. This potential issue is mitigated further from operating the chamber in SS mode whereby compound loss and re-evaporation quickly come to steady state. Short lifetimes of radical intermediates with other gas-phase constituents also render a negligible wall loss. The stability of BnOH in the chamber was investigated and BnOH was found to be highly stable, with results given in the Supplement (Sect. S1). Denuders and GF filter samples were also analyzed to probe reproducibility of the analytical technique. The analysis showed consistent results.

Gas and particle samples from BnOH photooxidation are dominated by oxygenated species, several not having authentic standards, and thus a portion of each sample was derivatized. Initially, we eliminated peaks detected in blank and background samples. For compounds having standards, comparisons were made between the retention times and mass spectra (CI and/or EI mode) of the chamber-derived peaks and those of the standards. For compounds not having standards, individual peak identifications were associated with a product peak only if its retention time and mass spectrum were consistent with the fragmentation pattern of the BSTFA-derivatized compound. All recorded spectra in this study were compared with those derived from reference standards, the literature, the NIST library, and an archive of mass spectra from product compounds determined in our laboratory over the past 20 years.

3 Results and discussion

The initial conditions of the experiments conducted in this study are summarized in Table 1. Three NO_x experiments were carried out with initial BnOH ranging from 0.36–0.72 ppm and NO from 0.096–0.19 ppm. One experiment without NO_x was conducted with initial H_2O_2 and BnOH levels of 3.0 and 0.32 ppm, respectively. NO_x experiments were conducted at ~ 30 % RH and the H_2O_2 experiment at < 4 % RH to minimize H_2O_2 uptake onto chamber surfaces.

Table 1. Initial conditions for BnOH experiments in the presence and absence of NO.

Exp. IDs	BnOH (ppb)	H$_2$O$_2$ (ppm)	NO* (ppb)	Seed surface area (nm^2 cm^{-3})	BnOH / NO (ppb ppb^{-1})	T (°C)	RH (%)
ER889	385	–	178	4.67×10^7	2.2	24.5	31.0
ER890	355	–	96	4.94×10^7	3.7	24.5	31.1
ER891	723	–	188	9.88×10^7	3.8	24.6	31.3
ER892	319	3.04	–	1.36×10^6	–	25.7	< 4.0

T: temperature; RH: relative humidity. Seed aerosol at 1 µg m^{-3}. * The initial NO$_x$ during the irradiation was greater than 98 % NO.

Chamber temperatures were set to 25 °C. Each experiment was conducted for up to 5 d for samples requiring substantial masses or extended collection times and frequencies.

Steady-state concentrations of NO, BnOH, O$_3$, and NO$_y$ for the four experiments are given in Table 2. The reacted BnOH and NO were calculated from the difference between the initial and steady-state concentrations. For NO$_x$ experiments, the range of reacted BnOH concentrations was 0.22–0.34 ppm, having a reproducibility of 20 %–30 %. Under these conditions, steady-state concentrations of NO$_y$ and O$_3$ were in the range of 0.08–0.16 and 0.011–0.15 ppm, respectively. With NO present at steady state, peroxy–peroxy (RO$_2$–RO$_2$) reactions were minimized. A constant aerosol source was maintained for initial conditions given in Table 1. The major aerosol parameters measured (SOA, SOC, and OM/OC) are given in Table 3. SOC uncertainties were taken from the reproducibility of the semi-continuous measurement and were typically better than 10 % for a single run. For the organic mass (OM), the uncertainties are determined from the reproducibility of side-by-side filter measurements, which are typically better than 5 %. An estimate of the systematic errors due to minor changes in reactant concentrations, minor variations in chamber temperature, and similar factors brings the total uncertainty to 15 %–25 % for these parameters (Kleindienst et al., 2009). SOA / SOC values were then determined from the corrected data and are given in Table 3. For experiments in the presence of NO$_x$, SOA / SOC values ranged from 1.7–2.0. Similarly, in the absence of NO$_x$, the measured SOA / SOC value was 2.1.

3.1 Secondary organic aerosol and secondary organic carbon yields

Secondary organic aerosol yield (Y_{SOA}) and secondary organic carbon yield (Y_{SOC}) were calculated from the following respective relationships:

$$Y_{SOA} = SOA/\Delta HC, \tag{1}$$
$$Y_{SOC} = SOC/\Delta HC_C, \tag{2}$$

where SOA is the corrected organic aerosol mass concentration originating from filter measurements (six filters) and ΔHC is the reacted BnOH concentration. SOC is the organic

carbon concentration found in Table 3 and ΔHC_C is the reacted BnOH carbon concentration. SOA and SOC were corrected for wall loss to the chamber, which had previously been determined for organic aerosol to be 0.067 h^{-1} (Kleindienst et al., 2012). The wall loss rate is based on mass and not on the size distribution of the particles. Uncertainties in the yield come from the experimental uncertainties in SOA and SOC production and the reacted BnOH concentrations. The uncertainty in the reacted BnOH results from the reproducibility of the initial and steady-state values and is estimated to range from 20 %–30 % given the low volatility of BnOH and challenges for introducing oxygenated species into the chamber in a consistent manner. Such challenges are also present in a batch mode experiment given the difficulty to determine BnOH time profiles given its volatility and high reactivity toward oxidants (Shilling et al., 2008; Kroll et al., 2007). Similar findings have been reported for sesquiterpene oxidation (Jaoui et al., 2013). As a result, aerosol yields of higher accuracy are often reported to be associated with steady state as opposed to batch mode experiments (Shilling et al., 2008). Moreover, in this work we explored the possibility of BnOH being taken up by ammonium sulfate (AS) seed aerosol prior to the start of the irradiation or by SOA after it is initiated. This test was conducted using GC-MS analysis of derivatized (BSTFA) and underivatized denuder and GF filter extracts collected before and after the reaction starts (Sect. S1). Under the experimental conditions used in this study, BnOH was undetected in AS and SOA, thus limiting any participation in particle chemistry that may occur.

The production of aerosol and thus the yield were found to be highly sensitive to the precise initial conditions (Tables 1 and 3). Yields for the four experiments are shown in Table 3. Y_{SOA} values were determined for SOA concentrations from 39.6–119.5 µg m^{-3} and ranged between 3.6 % and 8.1 %. Similarly, Y_{SOC} was measured for SOC concentrations from 23.2–58.9 µg C m^{-3} and found to range between 2.7 % and 5.1 %. In the absence of NO$_x$, SOA and SOC yields were 5.2 % and 3.1 % measured for SOA and SOC concentrations of 52.9 µg m^{-3} and 24.8 µg C m^{-3}, respectively. For the two systems at similar SOA concentrations ER890 and ER892, the SOA yield was higher for the experiment with NO$_x$. This may result from the reaction of BnOH with NO$_x$,

Table 2. Steady-state GP and reacted BnOH and NO concentration during the irradiation.

Exp. IDs	NO (ppb)	Reacted NO (ppb)	BnOH (ppb)	Reacted BnOH (ppb)	BnOH / NO ratio (ppb ppb^{-1})	O$_3$ (ppb)	NO$_y$ (ppb)
ER889	78	100	132	253	1.7	30	163
ER890	9	87	132	223	14.7	147	80
ER891	29	159	387	336	13.4	11	146
ER892	–	–	85	234	–	28	–

Table 3. Formation and yields of SOA (Y_{SOA}) and SOC (Y_{SOC}). All organic and carbon aerosol masses are corrected for a wall loss of $0.067\,h^{-1}$ (Kleindienst et al., 2012).

Exp. IDs	SOA ($\mu g\,m^{-3}$)	SOC ($\mu g\,C\,m^{-3}$)	SOA / SOC	Y_{SOA} (%)	Y_{SOC} (%)
ER889	39.6	23.2	1.7	3.6	2.7
ER890	56.1	30.3	1.9	5.7	4.0
ER891	119.5	58.9	2.0	8.1	5.1
ER892	52.9	24.8	2.1	5.2	3.1

which tends to produce high levels of BnAld (Table 4) that may undergo secondary reactions leading to additional SOA formation (see Sect. 3.3). The BnOH reaction with NO will occur when the reaction of RO$_2$ with NO is competitive to ring closure. Regardless, according to Wang (2015) the reaction of NO$_2$ with R1 (Scheme 1) will occur only to a minor degree compared with ring closure. As expected, the data in Table 3 indicate that Y_{SOA} and Y_{SOC} are lower at the lower SOA and SOC concentrations, respectively.

These SOA and SOC yields can be compared with other studies. Recently, Charan et al. (2020) reported SOA yields for the photooxidation of BnOH in the presence of NO$_x$ with the initial OH coming from the photolysis of H$_2$O$_2$. Their chamber was operated in a batch mode, and SOA yields approaching unity were reported. By contrast, three additional studies reported much lower SOA yields of 9 %, 30 %, and 41 %: McDonald et al. (2018), Carter et al. (2005), and Li et al. (2018), respectively. The yield reported by McDonald et al. (2018) was based on a multi-generation oxidation model; that of Carter et al. (2005) was estimated as described in the original report, and that of Li et al. (2018) was based on measurements in the presence of NO$_x$ and a surrogate urban hydrocarbon. The results of our study are much closer in value to McDonald et al. (2018). The study by Charan et al. (2020) suggests that conditions can be found under which BnOH SOA yields are substantially greater than that found in this study and those previously reported. The major differences between the Charan et al. (2020) study and the present work were the chamber mode operation, the seed aerosol type and levels, and the mix of oxidants used. While it can be difficult to compare the yields from the two studies some comments can be made. (1) As noted, the Charan et al. (2020) yields result from conventional batch mode irradiation of BnOH, H$_2$O$_2$, and NO$_x$. (2) SOA levels were measured using an

SMPS that measures aerosol volume, which is then converted to aerosol mass using a density of $1.4\,\mu g\,nL^{-1}$. (3) Perhaps the biggest difference between the two studies is the use of an extremely high initial seed aerosol mass, approximately 2 orders of magnitude higher than in this study. Thus, it is possible that an adsorption mechanism played a part in contributing to the measured yields. (4) Finally, the use of high initial H$_2$O$_2$ concentrations relative to BnOH makes it possible that H$_2$O$_2$ effectively competed with BnOH for OH via the reaction of OH + H$_2$O$_2$ → HO$_2$ + H$_2$O, thus generating a system rich in HO$_2$. Thus, the aging process may be more prominent than in our study. The uncertainties associated with SOA and reacted BnOH measurements as well as wall loss correction are unlikely to account for the differences in the two studies. However, SOA yields have been reported to increase considerably as a function of initial seed aerosol (Zhang et al., 2014), as well as to increase with the OH radical exposure (Wang et al., 2018). Qualitatively these two factors might bring the present SOA yields into reasonable agreement with Charan et al. (2020) if data were extrapolated to similar seed aerosol and OH exposures. And as previously noted, in the low initial seed aerosol used in our study no benzyl alcohol was detected in the seed aerosol or deposited on SOA. As further support for the plausibility of the results from the present study, Humes et al. (2022) recently reported yields from 12 %–18 % for two oxygenated aromatic species (1-phenoxy-2-propanol, and phenoxy-ethanol), which are compounds with structures similar to BnOH.

3.2 Reaction product identification

Three methods were used in this study to identify oxygenated reaction products at the molecular level: (1) DNPH as the derivatizing agent for small carbonyls (Smith et al., 1989),

Table 4. Steady-state carbonyl concentrations (ppmV) during BnOH oxidation (FH: formaldehyde; AH: acetaldehyde; Ac: acetone; MA: methacrolein; BN: 2-butanone; BnAld: benzaldehyde; G: glyoxal; MG: methylglyoxal).

Exp. ID	FH	AH	Ac	MA	BN	BnAld	G	MG
ER889	2.4	1.2	1.0	1.0	0.6	23.09	5.0	0.6
ER890	1.5	2.8	–	–	2.9	18.2	3.8	0.4
ER891	5.1	2.5	1.3	2.0	1.4	30.8	8.6	0.6
ER892	181.7	23.5	–	0.8	0.8	5.2	7.8	1.6

(2) BSTFA as the derivatizing agent for hydroxyl and carboxylic compounds for GP and PP (Jaoui et al., 2004), and (3) the direct injection (DI) method providing the capability for analyzing slightly polar to non-polar compounds without the use of derivatization (Jaoui and Kamens, 2001). For the BSTFA and DI methods, the analysis of laboratory-generated GP and PP products from BnOH oxidation shows a series of organic compounds containing nitro, ketone, carboxylic acid, and/or alcoholic functional groups. Many of these compounds do not have authentic standards and their identifications were based on the interpretation of the mass spectra of the derivatized and/or underivatized compound (Jaoui and Kamens, 2001; Jaoui et al., 2004, 2005). The identification should be regarded as tentative except for compounds that have authentic standards. For the BSTFA method, the recognition of characteristic ions was used to guide the analysis of mass spectra of the derivatives obtained in both electron ionization (EI) and chemical ionization (CI) using methane as the reagent gas. BSTFA reacts with -COOH and -OH groups to form BSTFA derivatives. Characteristic ions are m/z 73, 75, 147, and 149. Adduct ions in CI from the derivatives include m/z $M^{+\bullet} + 73$, $M^{+\bullet} + 41$, $M^{+\bullet} + 29$, and $M^{+\bullet} + 1$; fragment ions include m/z $M^{+\bullet} - 15$, $M^{+\bullet} - 73$, $M^{+\bullet} - 89$, $M^{+\bullet} - 117$, $M^{+\bullet} - 105$, $M^{+\bullet} - 133$, and/or $M^{+\bullet} - 207$. The approach used for the identification is as follows: peaks detected in blank and background chamber samples were eliminated first. A peak was associated with a reaction product only if its corresponding mass spectrum was consistent with the fragmentation pattern of the BSTFA derivatization reagent. All recorded spectra were compared with spectra derived from various reference compounds, authentic standards, the NIST library, the PubChem website (http://pubchem.ncbi.nlm.nih.gov, last access: 14 September 2022), and/or by MS assignment. While the offline technique is an integrated technique that requires long sampling times, it does provide a sensitive method for product identification at the molecular level as well as measuring low concentrations of highly oxidized organic compounds and semivolatile compounds in the GP. Thus, products found by this collection technique could be informative for possible precursors for the types of compounds that may form in the PP. In the following discussion, data are first presented to support tentative identifications of oxidation products in the GP and PP.

3.2.1 Gas-phase products

GP measurements were made of major carbonyl products formed during the photooxidation of BnOH including formaldehyde, acetaldehyde, acetone, methacrolein, 2-butanone, BnAld, glyoxal, and methylglyoxal. Steady-state concentrations are given in Table 4. Under the conditions shown in Tables 1 and 2, high concentrations were observed for BnAld and glyoxal, and to a lesser extent formaldehyde in experiments with NO_x, as were high concentrations of formaldehyde, acetaldehyde, and to a lesser extent BnAld and glyoxal in the experiment without NO_x. BnAld level was a factor of ~ 5 higher in NO_x experiments compared to H_2O_2 experiments and formaldehyde a factor of ~ 36 lower. Glyoxal and methylglyoxal concentrations were largely similar in both NO_x and H_2O_2 experiments. The formation of BnAld, glyoxal, and formaldehyde as major products (Table 4) has already been reported from the oxidation of BnOH with yields of 25 (± 5), 20 (± 2), and 3.0 % (± 0.2), respectively (Bernard et al., 2013; Harrison and Wells, 2012).

GP samples were also collected on five-channel annular denuders. Each denuder sample was extracted and analyzed directly with GC-MS without derivatization. The remaining extract was silylated and GC-MS analyzed qualitatively. Typical total ion chromatograms (TICs) of GP products detected and identified in this study are shown in Fig. 1. Figure 1 shows portions of three TICs in +EI of GP samples taken from experiments ER889 at steady state (underivatized: Fig. 1a), ER892 (underivatized: Fig. 1b), and ER889 (silylated derivatives: Fig. 1c). Peaks assigned in Fig. 1 were identified either by comparison with an authentic standard or by MS assignment. For clarity, only the main products are shown, although several peaks could not be structurally identified. SOA generated from BnOH photooxidation is dominated by oxygenated ring-opening products (see below). However, ring-retaining products were among the main products observed in the GP including semivolatile organic compounds (SVOCs) (Fig. 1c). Chromatograms associated with the underivatized samples (Fig. 1a and b) were used mainly to identify BnOH and BnAld in the system, although several additional peaks absent in the background chromatogram were observed. At steady state, BnOH was not reacted completely as it was detected in both systems only in the GP using both DI and BSTFA methods (Fig. 1). BnAld was detected in both systems in the gas and particle phases, al-
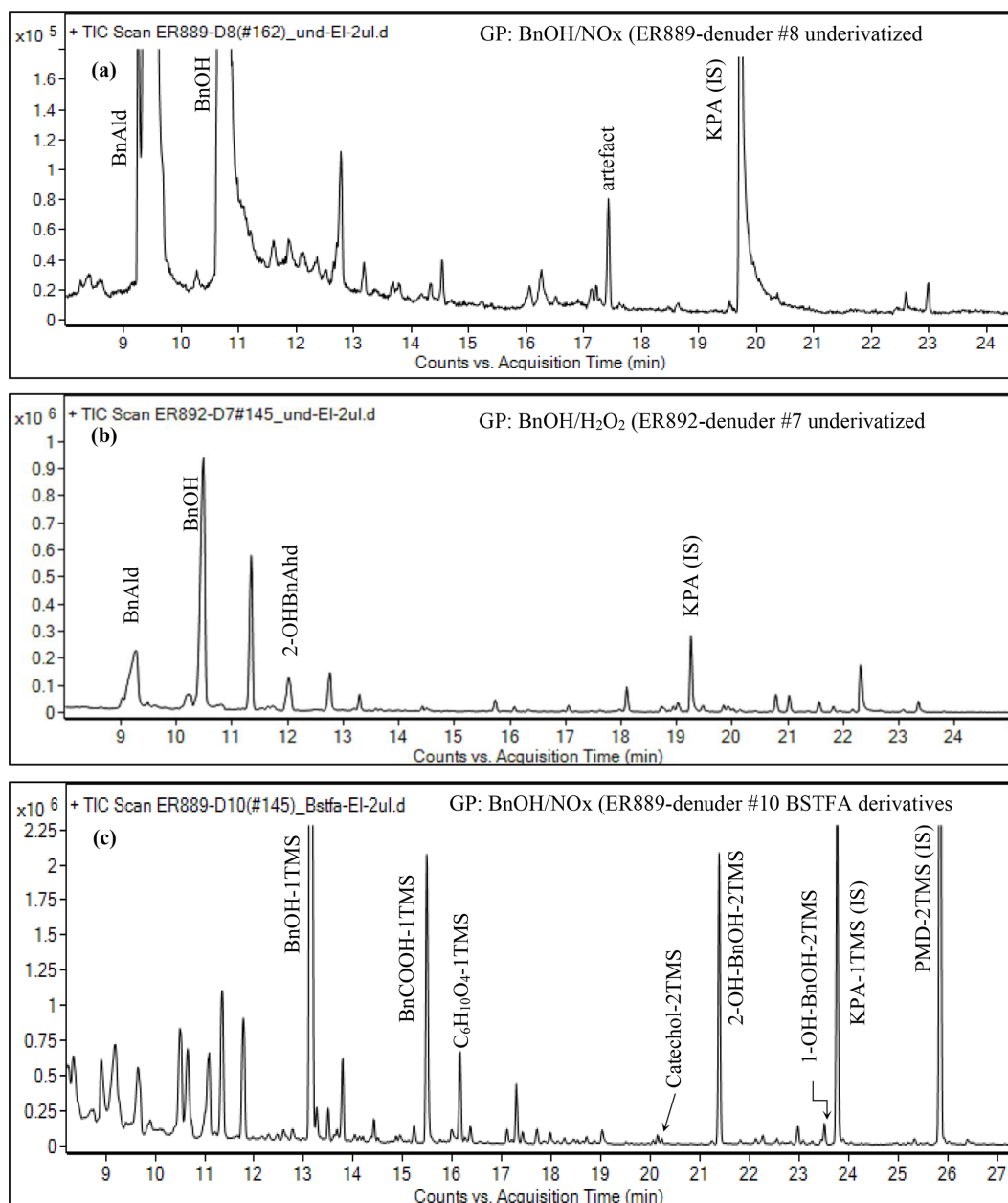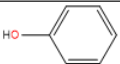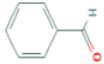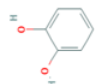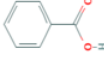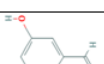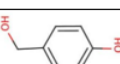
Figure 1. Portion of GC-MS total ion chromatogram in EI mode of GP underivatized denuder extract **(a)** ER889 (presence of NO$_x$), **(b)** ER892 (absence of NO$_x$), and **(c)** ER889 (presence of NO$_x$) as BSTFA derivatives.

though it was not present with the BSTFA method because of the absence of OH or COOH groups. Figure S3 shows EI mass spectra of BnAld identified using authentic standards and those associated with three peaks eluting at 11.3, 12.0, and 12.8 min. Although no structural information could be associated with these three peaks, molecular weights of 152, 152, and 138 Da were tentatively obtained; the unit for all derivatized and underivatized masses is the dalton (Da), but this is not designated as such hereafter.

Select GP products containing OH groups identified in the present study are summarized in Table 5. Table 5 con-

tains proposed structures, molecular weights of the silylated derivatives (MW$_{BSTFA}$) and underivatized compounds (MW), formulas, and the five most intense ions associated with BSTFA derivatives in EI mode. Table 5 shows if GP products are also detected in the PP. Figure S4 shows EI mass spectra associated with selected peaks observed in Fig. 1c, including BnOH-1TMS (trimethylsilane), benzoic acid-1TMS, catechol-2TMS, and 2-hydroxybenzyl alcohol-2TMS. The 2-hydroxybenzyl alcohol-2TMS (2OHBnOH) peak eluted at 21.4 min was one of the largest peaks detected in the chromatogram in Fig. 3c. The 2OHBnOH-2TMS EI

Table 5. Summary of selected reaction products detected and identified in either the gas phase (GP), particle phase (PP), or both from BnOH / NO$_x$ and BnOH/H$_2$O$_2$ experiments. Tables 6 and 7 show additional aerosol species with a high oxygen-to-carbon ratio and/or nitro group. N/a: not applicable. [a] Underivatized m/z values are given. [b] Identified with an authentic standard.

IUPAC/common nomenclature	Formula	m/z BSTFA (EI)	MW [MW$_{BSTFA}$] (g mol^{-1})	Proposed Structure	Detected
Benzyl alcohol (BnOH)	C$_7$H$_8$O	165, 91, 135, 180, 73	108 [180]		GP
Phenol	C$_6$H$_6$O	73, 151, 166, 94, 65	94 (166)		GP, PP
Benzaldehyde (BnAld)	C$_7$H$_6$O	106, 105, 77, 77, 51	106 (NA)		GP, PP
Benzene-1,2-diol (catechol)	C$_6$H$_6$O$_2$	239, 255, 80, 283, 73	110 (254)		PP
Benzoic acid	C$_7$H$_6$O$_2$	179, 105, 135, 77, 194	122 (194)		GP, PP
Salicylaldehdye	C$_7$H$_6$O$_2$	179, 105, 135, 77, 194	122 (194)		GP
3-Hydroxy benzaldehyde	C$_7$H$_6$O$_2$	179, 105, 135, 77, 194	122 (194)		GP
2-Hydroxybenzyl alcohol (salicyl alcohol)	C$_7$H$_8$O$_2$	73, 253, 179, 268, 147	124 (268)		GP, PP
4-Hydroxybenzyl alcohol	C$_7$H$_8$O$_2$	73, 179, 253, 268, 147	124 (268)		GP, PP
4-Hydroxybenzoic acid (p-salicylic acid)	C$_7$H$_6$O$_3$	267, 223, 193, 282, 73	138 (282)		PP [H$_2$O$_2$]

mass spectrum (Fig. S4, bottom) shows strong characteristic fragments ions at m/z 73, 179 (M$^{+\bullet}$ − 89), 253 (M$^{+\bullet}$ − 15), and 268 (M$^{+\bullet}$), and its corresponding CI mass spectrum shows ions at m/z 253 (M$^{+\bullet}$ − 15), and 179 (M$^{+\bullet}$ − 89) and weak adducts at M$^{+\bullet}$ + 1, M$^{+\bullet}$ + 29, and M$^{+\bullet}$ + 41 that are consistent with the presence of two (-OH) groups, indicating a BSTFA derivatized molecular weight of 268 Da. Bernard et al. (2013) have identified 2OHBnOH and catechol in the GP of the reaction of BnOH and OH radicals. In our study, catechol was observed only in the H$_2$O$_2$ system in the PP. Additional peaks were observed, the mass spectra of which are consistent with products bearing -OH groups and/or -COOH groups; however, their structural identification could not be obtained due to lack of authentic standards and the complexity of the interpretation of their mass spectra. BnAld was re-

ported to undergo secondary reactions (Sankar et al., 2014) and may play an important role as a precursor for some oxygenated species observed in this study.

3.2.2 Particle-phase products

One of the advantages of conducting experiments in SS mode is collecting sufficient gas and aerosol masses on denuders and filters for qualitative and quantitative offline analysis. In this study, aerosols collected on GF filters were solvent-extracted, with the resulting extracts subjected to BSTFA derivatization followed by GC-MS analysis. SOA generated from both NO$_x$ and H$_2$O$_2$ systems was dominated by oxygenated organic compounds, for which mass spectra for more than 50 species have been recorded. These species may
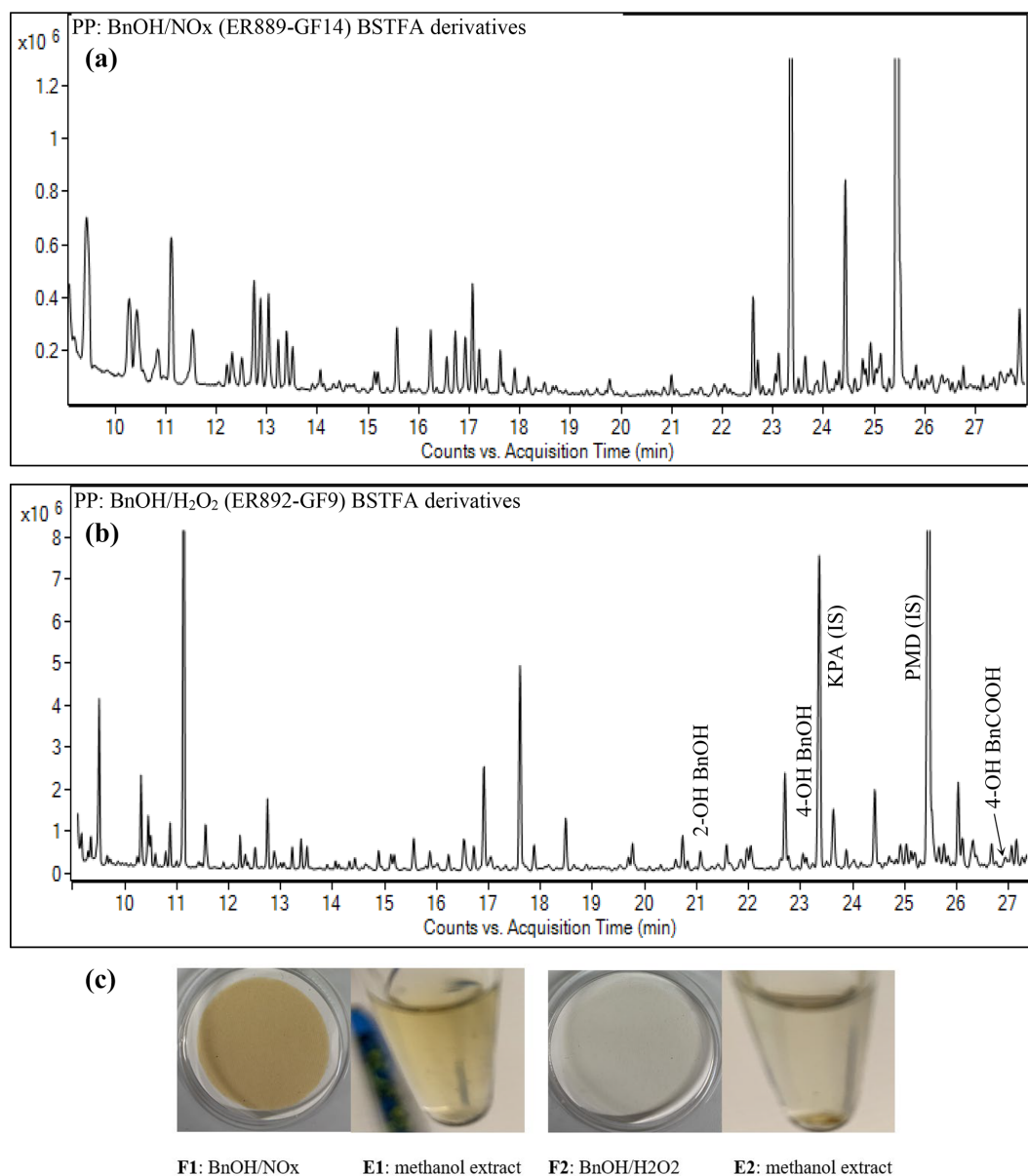
Figure 2. Portion of GC-MS total ion chromatograms (EI mode) of particle-phase extracts: **(a)** BSTFA derivatized sample from ER889 (presence of NO_x), **(b)** BSTFA derivatives from ER892 (absence of NO_x), and **(c)** the effect of mixture changes in filter and methanol extract appearance – BnOH / NO_x filter (F1) and BnOH/H_2O_2 (F2). The same volume of air was sampled on each filter.

have undergone several generations of atmospheric oxidation. Several individual large peaks have been detected in addition to a significant number of small peaks as shown in Fig. 2. Figure 2 shows portions between 9 and 28 min of the TICs of the silylated derivatives of the aerosol extracts associated with BnOH / NO_x (top) and BnOH/H_2O_2 (bottom). The portion after 28 min is discussed in the next section. The chromatograms in Fig. 2 can be directly compared because the chamber air sampled and the amount of extract analyzed for each system were the same. This evaluation revealed that more than 70 % of peaks eluted from each system are iden-

tical, suggesting similar chemistry is involved in BnOH reaction products formed in the presence and absence of NO_x. In addition, a series of peaks dominated by fragments with odd m/z were observed only in BnOH / NO_x, and their mass spectra were associated with nitrogen-containing compounds as discussed in the section on NACs. This suggests that the composition of a portion of SOA produced in the presence of NO_x is different than that formed in the absence of NO_x, which can be clearly illustrated by the filter and extract color shown in Fig. 2 (bottom). Consistent with the presence of nitro-aromatics, filter F2 and methanol extract (E2) has lost

most of the color seen in F1 and E1. The presence of NO_x in the system produced material (filter F1) of a deep brown color. Most species structurally identified in this study have not been reported in the literature, and mass spectra associated with several peaks are provided either in the main paper or in the Supplement. Additional reaction products (e.g., oligomers, organonitrates) might have been present in the SOA but could not be detected based on the analytical techniques used in this study. Note that formulae, in particular chemical structure, could not be obtained for several peaks recorded in this study due to challenges interpreting their mass spectra. A set of compounds identified and detected before 28 min in the present study are summarized in Table 5.

Ring-retaining products (e.g., 2-hydroxy benzyl alcohol, benzoic acid, 4-hydroxy benzoic acid, and catechol) were detected in the PP in both systems. As noted above, some ring-retaining products were also detected in the GP as shown in Table 5. Salicylaldehyde and 3-hydroxybenzaldehyde were present only in the GP. These two hydroxy-aldehydes may undergo additional secondary reactions, leading to some ring-opening products observed in this study. Representative EI mass spectra of the TMS derivatives associated with four compounds are shown in Fig. 3 including benzoic acid, benzene-1,2-diol (catechol), 4-hydroxybenzoic acid, and 2-hydroxybenzyl alcohol. Additional EI and CI mass spectra are shown in Figs. S4 and S5 in the Supplement. The EI mass spectrum of the BSTFA derivative of 2-hydroxybenzyl alcohol displayed in Fig. 3 shows abundant fragment ions at m/z 73, 147, 267 ($M^{+\bullet}$), 253 ($M^{+\bullet}-15$), and 179 ($M^{+\bullet}-89$) and weak ions at m/z 91, 223, and 163. The corresponding CI mass spectrum displayed in Fig. S4d shows abundant fragment ions at m/z 268 ($M^{+\bullet}$), 253 ($M^{+\bullet}-15$), and 179 ($M^{+\bullet}-89$) and adduct ions at m/z 293 ($M^{+\bullet}+29$) and 309 ($M^{+\bullet}+41$). This fragmentation pattern is consistent with the presence of a compound with two hydroxyl groups and a benzene ring (m/z 91) having molecular weight 268 for the BSTFA derivative and MW 124 for its underivatized form. Similarly, the BSTFA EI mass spectrum of 4-hydroxybenzoic acid (Fig. 3c) shows characteristic fragment ions at m/z 73, 193 ($M^{+\bullet}-89$), 223 ($M^{+\bullet}-60$), 267 ($M^{+\bullet}-15$), and 282 ($M^{+\bullet}$), and its CI mass spectrum shows fragment ions at m/z 73, 193, and 67 and adducts at 283 and 311. Again, these fragments and adducts are consistent with the presence of two (-OH) groups and a molecular weight of the derivatized compound of 282 and 138 for the underivatized compound. The presence of a peak at m/z 153 ($M^{+\bullet}-117$) is consistent with a compound bearing an organic acid group. The EI mass spectra recorded in this study for 2-hydroxybenzyl alcohol and 4-hydroxybenzoic acid are identical to the reference NIST spectrum (http://webook.nist.gov, last access: 14 September 2022). Figure S5 shows EI mass spectra associated with four peaks eluted at 12.86, 15.58, 16.24, and 19.78 min consistent with the fragmentation pattern of BSTFA derivatives, although their structures could not be obtained.

3.2.3 Highly oxygenated compounds (HOCs)

Recent studies show that highly oxygenated compounds (e.g., HOMs) play an important role in understanding SOA formation (Berndt et al., 2016; Jaoui et al., 2019, 2021, and references therein, Piletic and Kleindienst, 2022). These compounds may result from several generations of atmospheric oxidation. In this study, several ring-opening products that eluted late in the chromatograms (RT > 25 min), with a relatively high O : C ratio of > 1.3 likely contributing to their condensation in the PP, were detected. Three groups of these oxidation products were detected in the PP in both systems. Figure 4 shows the portion between 25 and 34 min of selected GC-MS extracted ion chromatograms, where these groups (color-coded) elute, and uses the selected ions m/z 423, 437, and 525 (merged in one chromatogram) to best illustrate them: (a) BnOH / NO_x, (b) BnOH/H_2O_2, (c) chamber background. Groups 1, 2, and 3 consist of three (green), eight (blue), and four (red) peaks, respectively, and are completely absent from the background chromatogram (Fig. 4c). Results from a comprehensive interpretation of EI and CI mass spectra associated with peaks shown in Fig. 4 enabled the identification of several isomers associated with each group. Figure 5 displays three EI mass spectra associated with each group main peak, along with proposed structure and chemical formulae. Table 6 gives the major highly oxygenated compounds identified in this research, including the main peaks from each of these groups, in the order of their underivatized molecular weight. Table 6 gives the chemical formulas, O : C mass ratio, the five most abundant ions associated with each TMS derivative in methane CI and EI modes, the molecular weights of the underivatized (MW) and TMS derivatized compounds (MW$_{BSTFA}$), and the proposed chemical structures of the compounds.

Group 1 consists of *meso*-tartaric acid (*m*TA) (Rt 26.04 min) and *L*-/*D*-tartaric acids (*l*TA/*d*TA) (Rt 27.66 min) identified based on authentic standards. The mass spectra of BSTFA derivatives of *l*TA and *d*TA standards (Fig. S6, Supplement) are very similar (eluting at the same time) and are only slightly different from the *m*TA (Fig. S6); however, *l*TA–*d*TA and *m*TA elute at two different retention times (Figs. 4, S6). The peaks associated with *m*TA and *l*TA–*d*TA are among the largest peaks observed in this portion of the chromatograms. Note that the *l*TA isomer is the most abundant tartaric acid present in nature (DeBolt et al., 2006). The fragments and adducts observed for the peak eluting at 25.19 min are similar to those of mTA and *d*-/*l*TA and are consistent with the presence of four OH groups, a MW of 452 for the derivatized compound and 164 for the underivatized compound, and a $C_4H_6O_6$ chemical formula. Tartaric acid has been reported in ambient aerosol (Röhrl and Lammel, 2002; Gowda et al., 2016) and in chamber 1,3-butadiene SOA (Jaoui et al., 2014). Recent studies suggest that tartaric acid and other hydroxy carboxylic acids undergo heterogeneous OH reaction in aqueous solution, with the presence and
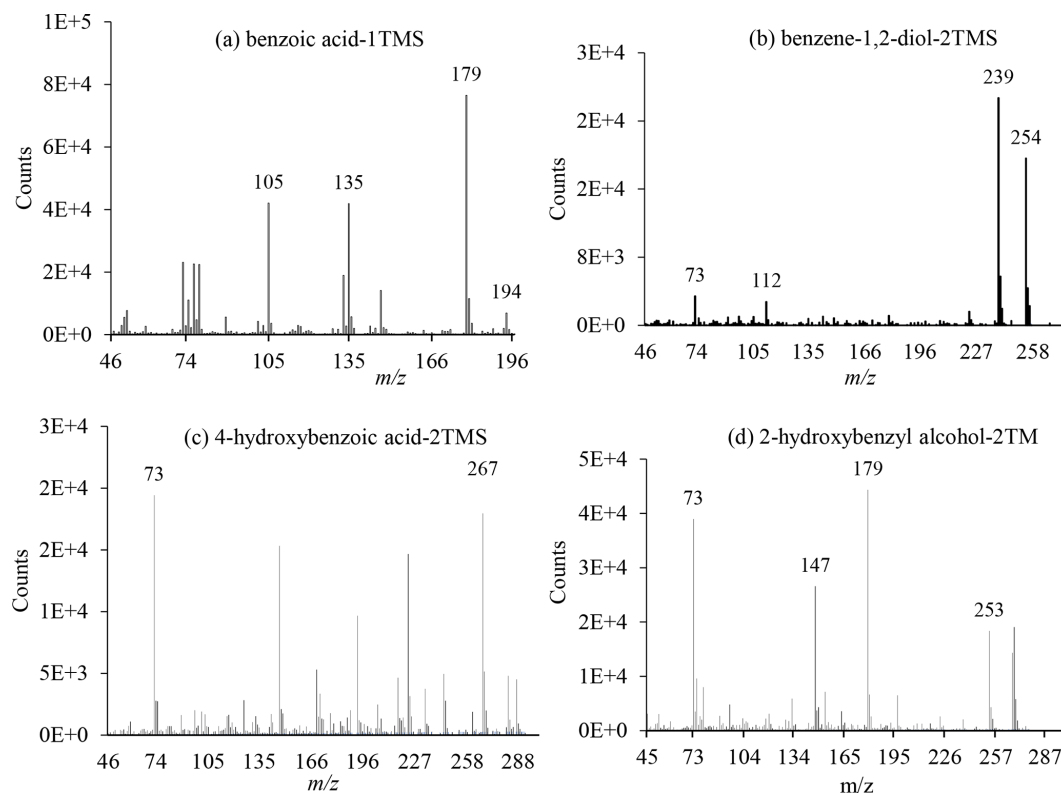
Figure 3. Positive EI mass spectra of BSTFA derivatives of selected ring-containing products: benzoic acid, benzene-1,2-diol, 4-hydroxybenzoic acid, and 2-hydroxybenzyl alcohol.
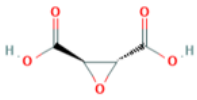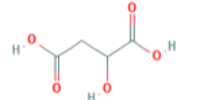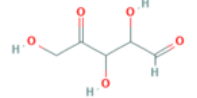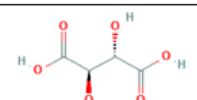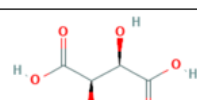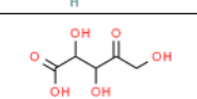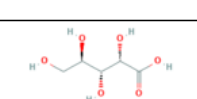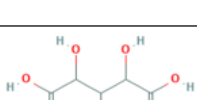
position of the OH group(s) playing an important role in fragmentation and functionalization of organic aerosol (Cheng et al., 2016).

Group 2 consists of eight peaks (Fig. 4: blue) eluting between 28.5 and 31.5 min. The EI and CI mass spectra associated with each peak display similar fragment and adduct ions across the range of 50 to 600 Da. The interpretation of these mass spectra allows us to infer the molecular weight (MW) of the underivatized compounds as 164 and MW_{BSTFA} of 452 for the TMS derivatives. The BSTFA CI mass spectrum of the peak eluted at 29.48 (largest peak) shows characteristic fragment ions at m/z 73, 437 $[M^{+\bullet}$ -15], 363 $[M^{+\bullet}$ - 89], and 305 $[M^{+\bullet}$ - 105] and an adduct at 453 $[M^{+\bullet}+1]$, 481 $[M^{+\bullet}+29]$, and 493 $[M^{+\bullet}+41]$. These fragments and adducts are consistent with the presence of four OH groups and an MW of 452 for the derivatized compound and 164 for the underivatized compound. The presence of peaks at m/z 347 $[M^{+\bullet}-105]$ and 335 $(M^{+\bullet}-117)$ is consistent with a compound bearing alcoholic and carboxylic OH groups simultaneously. This mass spectrum is similar to the one from methyltartaric acid reported previously from isoprene oxidation by our group (Jaoui et al., 2019). The silylated methyltartaric acid mass spectrum (Jaoui et al., 2019) and mass spectra associated with group 2 are only slightly different; however, they elute at different retention times. The peaks have been

tentatively identified as isomers of trihydroxy-oxo-pentanoic acid, with the structure of the 4-oxo-*D*-arabonic acid isomer shown in Table 6.

Group 3 consists of four peaks eluting between 32.5 and 34 min (Fig. 4: red). The EI and CI mass spectra associated with each peak display similar fragment and adduct ions across the range of 50 to 600 Da. As a descriptive example, an EI mass spectrum is shown in Fig. 5 for a peak eluted at 33.1 min. A comprehensive interpretation of EI and CI mass spectra associated with group 3 peaks (Figs. 4, 5) allows us to infer the molecular weight (MW) of the underivatized compounds as 180 and MW_{BSTFA} of 540 for the TMS derivatives, with a chemical formulae $C_5H_8O_7$. The compounds corresponding to these four peaks were identified as isomers of C_5-trihydroxydicarboxylic acids. This identification is tentative due to the absence of authentic standards, except for the peak eluting at 33.47, which was identified as pentaric acid (Table 6) based on authentic standards. The spectra of BSTFA derivatives of the remaining three red peaks are only slightly different from the pentaric acid spectrum (Fig. 6); however, they elute at different retention times. The EI mass spectra are also similar to those reported in the literature for a set of C5-aldaric acids and TMS derivatives including xylaric, arabinaric, and ribaric acids (Hinton, 2008; https://pubchem.ncbi.nlm.nih.gov, last access: 14 Septem-

Table 6. Highly oxygenated products (O : C > 1.3) identified in benzyl alcohol photooxidation in the presence of NO_x or H_2O_2. * Identified with an authentic standard. *L*-Tartaric acid and *D*-tartaric acid co-elute. The structures of the 4-oxo-*D*-arabonic acid isomer and 2,3,5-trihydroxy-4-oxopentanal isomer are shown for trihydroxy-oxo-pentanoic acid and trihydroxy-oxo-pentanal, respectively. Four peaks with similar fragments and/or adducts as pentaric acid were observed.

Nomenclature	Chemical Formulae	O/C Ratio (by wt)	m/z BSTFA Derivative (CI-CH4); (EI)	MW (MW_BSTFA)	Proposed Structure
Epoxysuccinic acid (2 peaks)	$C_4H_4O_5$	1.7	187, 261, 73, 277, 173 73, 173, 261, 129, 143	132 (276)	
2-Hydroxybutanedioic acid* (malic acid)	$C_4H_6O_5$	1.7	233, 335, 73, 307, 351 73, 147, 233, 245, 335	134 (350)	
Trihydroxy-oxo-pentanal (5 peaks)	$C_5H_8O_5$	1.3	73, 275, 203, 349, 393 147, 73, 349, 233, 259	148 (364)	
meso-Tartaric acid*	$C_4H_6O_6$	2.0	423, 321, 277, 439, 73 73, 147, 292, 219, 423	150 (438)	
L-Tartaric acid*	$C_4H_6O_6$	2.0	423, 321, 277, 439, 73 73, 147, 292, 219, 423	150 (438)	
Trihydroxy-oxo-pentanoic acid (8 peaks)	$C_5H_8O_6$	1.6	73, 437, 363, 481, 493 217, 73, 147, 437, 292	164 (452)	
D-Arabinonic acid* (Arabic acid)	$C_5H_{10}O_6$	1.6	361, 217, 73, 435, 525 204, 437, 73, 147, 319	166 (526)	
Pentaric acid* (4 peaks)	$C_5H_8O_7$	1.9	525, 333, 407, 435, 73 73, 292, 189, 407, 525	180 (540)	

ber 2022). Figure 6 shows the structure of pentaric acid and its four isomers (panel a), the spectra associated with BSTFA derivatives of pentaric acid observed in BnOH SOA (panel b: EI mode, panel c: CI–CH4 mode), and a standard (panel d: EI mode). Figure 6 also shows the structure of the main fragments observed in BSTFA derivatives of pentaric acid in EI mode including m/z at 540, 525, 407, 292, 147, and 73 Da. Pentaric acid and its isomers (aldaric acids) are reported to be formed from the oxidation of aldopentose (Hinton, 2008; Derrien et al., 2018), but no evidence has been provided for its presence in SOA samples. In the present study, we successfully identified aldaric acids from the oxidation of BnOH in SOA samples.

3.2.4 Nitro-aromatic compounds (NACs)

NACs of secondary origin are a possible contributor to urban OA. They not only adversely affect human health and the environment but also impact aerosol optical properties and the atmospheric radiation balance. By understanding the sources of NACs in ambient particles and their chemical identities, we can evaluate their impact on the climate, environment, and human health. Recently, the analytical capabilities associated with BSTFA derivatization have been extended to NACs bearing hydroxyl and carboxylic acid groups (Jaoui et al., 2018). Mass spectra of most silylated NACs, especially methane CI, are highly specific, reproducible, and produce characteristic fragments useful in determining struc-
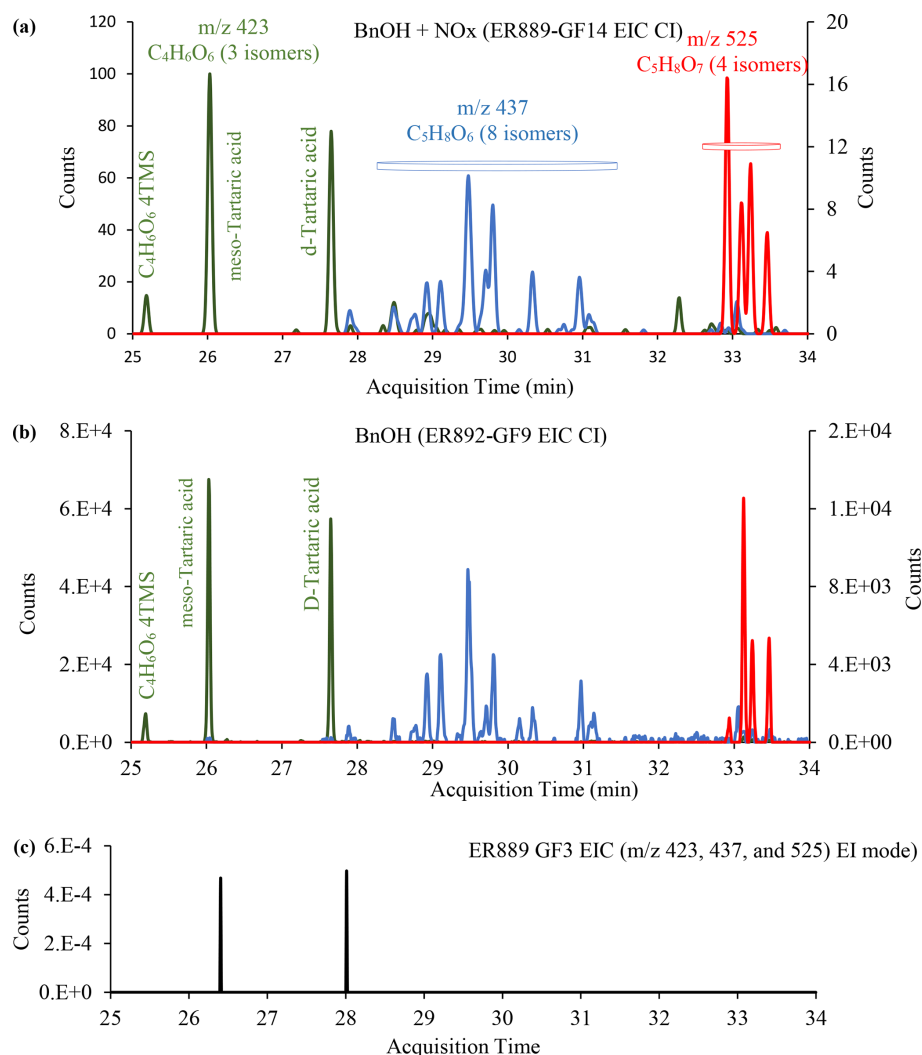
Figure 4. Portion (25–34 min) of GC-MS extracted ion chromatograms (CI–CH$_4$) at m/z 423 (green), m/z 437 (blue), and m/z 525 (red) merged in one chromatogram: **(a)** BnOH in the presence of NO$_x$; **(b)** BnOH in the presence of H$_2$O$_2$ and absence of NO$_x$. **(c)** Chamber background. Red and top blue: right axis.

tural information and molecular weight when authentic standards are not available (Jaoui et al., 2018). In this study, a detailed analysis of mass spectra associated with peaks in chromatograms (Fig. 1c for GP and Fig. 2, top, for PP) reveals the presence of several peaks presenting similar fragmentation patterns as those reported by Jaoui et al. (2018) for species bearing hydroxyl, carboxylic, nitro groups, and benzene ring. Figure 7 shows the portion between 23 and 42 min of two +EI extracted ion chromatograms for the BSTFA derivatives at m/z 210, 165 (IS), 299 (IS), 300, 298, 372, and 388 (merged into one chromatogram) associated with BnOH / NO$_x$ (top) and BnOH/H$_2$O$_2$ (bottom). The EI and/or CI mass spectra of selected nitro-aromatic standards can be found in Jaoui et al. (2018), and additional representative subsets of the derivatives are displayed in Fig. S7. For clarity, Fig. 7 inset shows an expanded portion of the top

chromatogram between 26.7 and 28 min. Table 7 contains proposed identification of NACs detected in this study, along with molecular weights, formulae, five main intense ions associated with CI and EI mass spectra of the derivatives, proposed structure, and the GP to PP peak area ratio.

NACs with the highest confidence assignment are those identified by comparing their retention times, EI, and CI mass spectra with those of reference standards. NACs with low levels of confidence are those (1) that have been previously identified in ambient PM or in smog chamber studies, (2) with EI mass spectra existing in the literature, or (3) with molecular weights and numbers of OH, COOH, and NO$_2$ groups that are simply consistent with the CI and EI mass spectrum (Jaoui et al., 2018). A total of 14 peaks associated with NACs were detected in this study. 3-Nitrobenzyl alcohol, 4-nitrocatechol, 2-hydroxy-5-
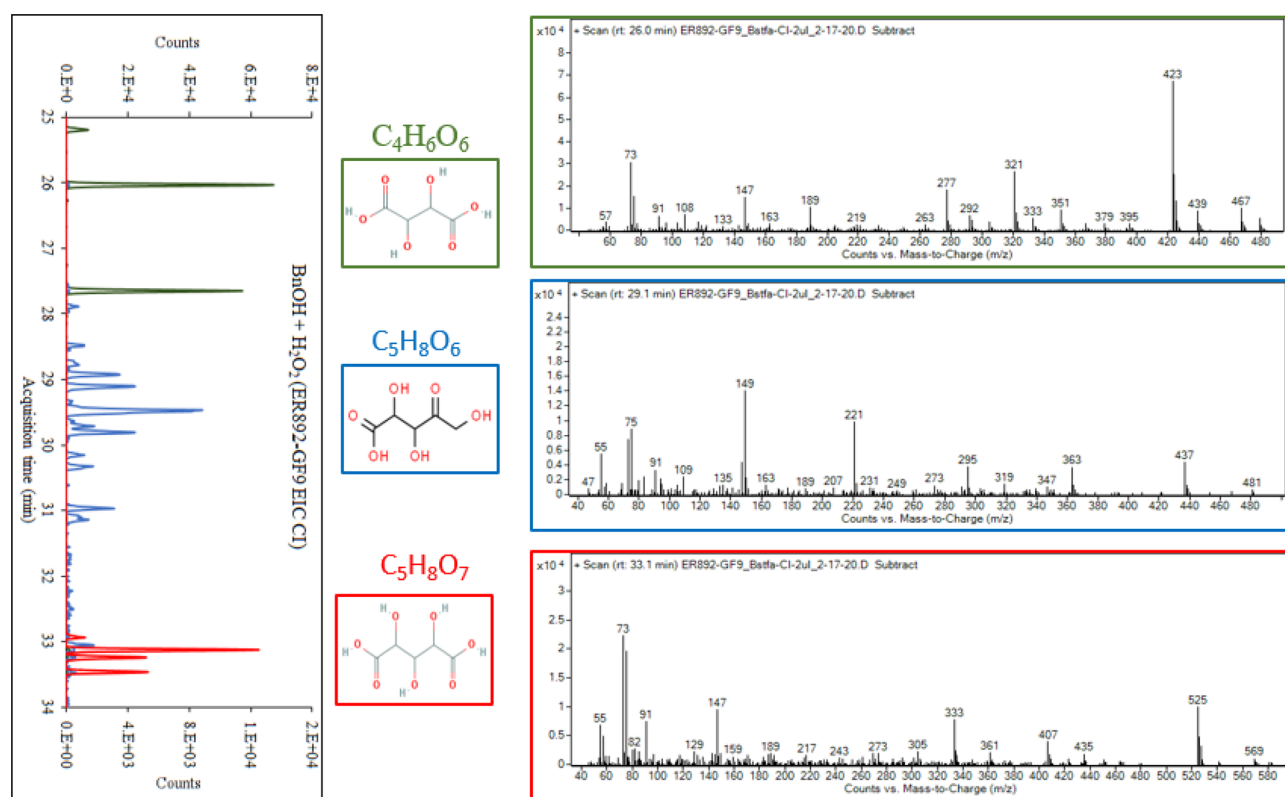
Figure 5. Mass spectra (methane CI) of ester TMS derivatives of meso-tartaric acid (top right), trihydroxy-oxo-pentanoic acid (middle right), and pentaric acid (bottom right), along with the portion of GC-MS extracted ion chromatograms shown in Fig. 6. Chemical formulae and chemical structure associated with each group are given in the middle column.

nitro benzyl alcohol, and 2-nitrophloroglucinol were identified based on authentic standards. Three peaks eluted at 33.76, 34.70, and 34.76 having similar mass spectra as 2-nitrophloroglucinol (main peak) eluted at 35.62 min were detected. They were tentatively associated with homologous series of 2-nitrophloroglucinol including 3-nitrobenzene-1,2,4-triol, 5-nitropyrogallol, and 4-nitro-1,2,3-benzenetriol (not shown in Table 7). Similarly, three additional peaks having similar mass spectra as 2-hydroxy-5-nitrobenzyl alcohol were observed and were tentatively associated with homologous series of 2-hydroxy-5-nitrobenzyl alcohol including 4-hydroxy-2-nitrobenzyl alcohol. The EIC in Fig. 7 (top) includes a series of four peaks observed only in the PP eluting at 35.94, 36.60, and 38.18 min, whose mass spectra were consistent with the presence of molecular weight 185 and 401 for the underivatized and derivatized compounds, respectively. Based on the similarity of their mass spectra, they were tentatively identified as structural homologues of 3,4-dihydroxy-5-nitrobenzyl alcohol (Table 7) with $C_7H_7NO_5$ formulae. As can be seen in Fig. 7 (bottom), NAC peaks were not detected in BnOH/H_2O_2 SOA extract, consistent with the formation of NACs in the presence of NO_x. All NACs were detected in both GPs and PP (Table 7), except 2-nitrophloroglucinol and 3,4-dihydroxy-5-nitrobenzyl alco-

hol, and their isomers were observed only in the PP, consistent with their low volatility. This result suggests that NACs may be formed in the GP and partition to the PP for those with low volatility, although PP reactions may occur as suggested by Charan et al. (2020), who analyzed only PP. 4-Nitrocatechol and 2-nitrophloroglucinol were among the largest NAC peaks observed in our study (Fig. 7). All three experiments conducted in this study were analyzed for NACs to probe reproducibility of the BSTFA method and showed consistent results. 2-Nitrophloroglycinol, 4-nitrocatechol, and other NACs have been reported in PM collected at Pico Mountain Observatory, Pico Island, in the Azores archipelago by Ikemori et al. (2019). A series of NACs has been reported recently by Charan et al. (2020) in BnOH SOA using offline UPLC/ESIQ-ToFMS (ultrahigh-performance liquid chromatography electrospray ionization quadruple time-of-flight mass spectrometry), and the structure assigned to formulas obtained from MassLynk software was based on expected oxidation products and MS/MS analysis. These observations support the identification of NACs reported in this study. 4-Nitrophenol was reported in the GP by Bernard et al. (2013) at low yield and by Charan et al. (2020) in SOA from the OH radical oxidation of BnOH but was not detected in either the GP or PP in this study.
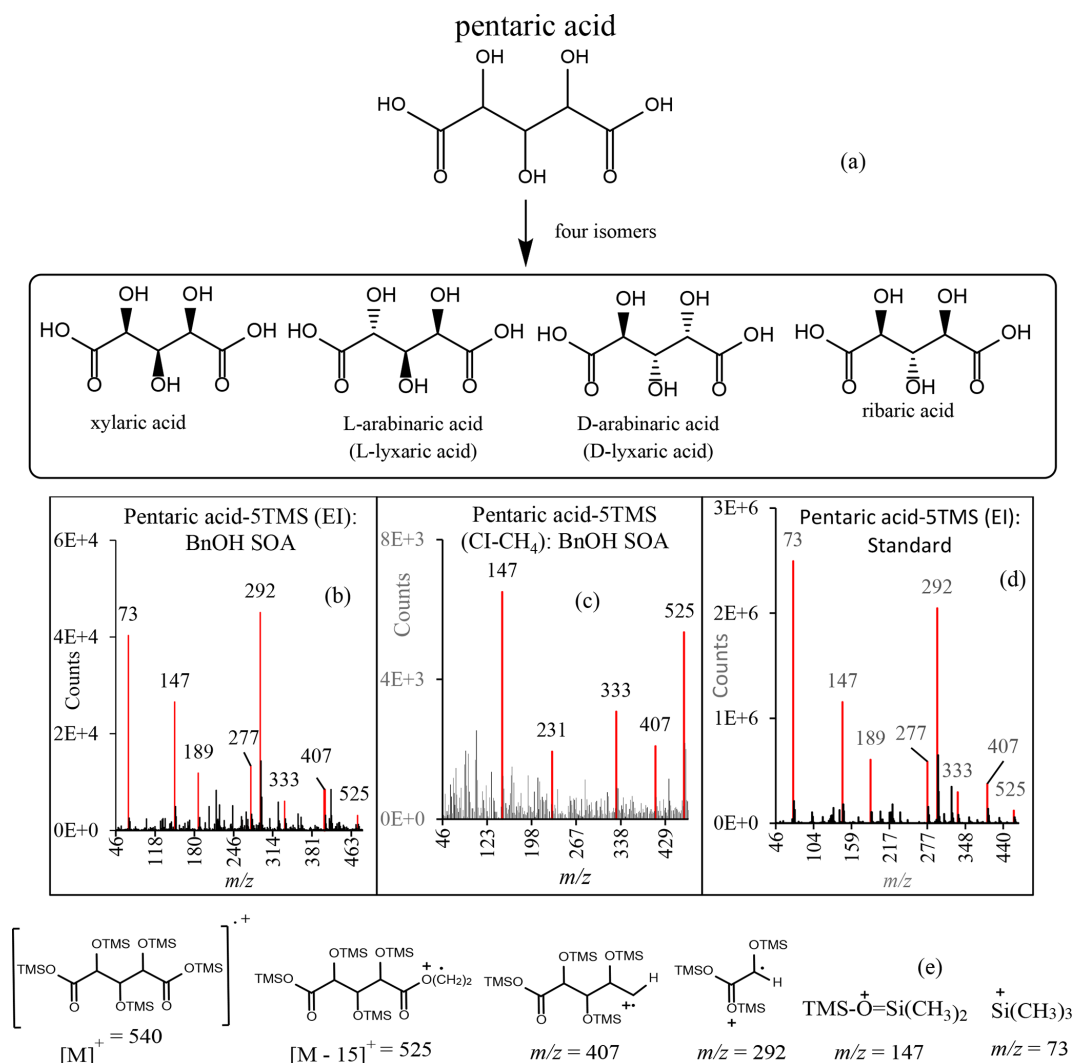
Figure 6. Molecular structures of pentaric acid and its isomers (**a**); mass spectra of TMS derivatives of pentaric acid acquired for smog chamber SOA (EI: **b**, CI: **c**) and an authentic standard (**d**: EI); major pentaric acid fragments observed in EI mode (**e**).

3.3 Mechanism of product formation

Based on known GP reactions for aromatic compounds, a schematic representation for the reaction of BnOH with OH is presented in Schemes 1–3. It is developed to understand the chemistry leading to the main GP and PP products identified experimentally in this study including HOCs and NACs. These schemes incorporate the latest experimental, quantum, and kinetic developments of the fate of peroxy–alkoxy benzoyl radicals including autooxidation (Wang, 2015; Sankar et al., 2014; and Namysl et al., 2020). The lines shown in these schemes are either one-step or multi-step pathways. Rate constants at room temperature of BnOH with the OH radical, O_3, and NO_3 radical of 2.8×10^{-11}, 6×10^{-19} (upper limit), and 4.0×10^{-15} cm^3 molecule^{-1} s^{-1}, respectively, have been reported in the literature (Harrison and Wells, 2009, 2012; Bernard et al., 2013). This suggests that the daytime oxida-

tion of BnOH will be mainly initiated by OH radicals. The reactions for O_3 and the NO_3 radical are not included in Schemes 1–3, although they are expected to be formed as minor products in our systems. Ozone is known to react primarily with compounds having double bonds and certainly not aromatic compounds. Ozone concentrations are low and given in Table 2. Likewise, the NO_3 reaction with aromatic compounds tends to be very slow and unlikely to have any impact in these systems. Moreover, given the $O_3 + NO_2$ reaction, NO_3 would only react with BnOH to a negligible degree.

The reaction of BnOH with OH radicals is initiated primarily by H atom abstraction from the external CH$_2$ group leading to BnAld and OH addition to the aromatic ipso (C1) and ortho (C2 or C6) positions to form two alkyldihydroxy adducts R1 and R2 (Scheme 1). The OH addition to the para (C3, C5) and meta (C4) position was reported to be unfavor-
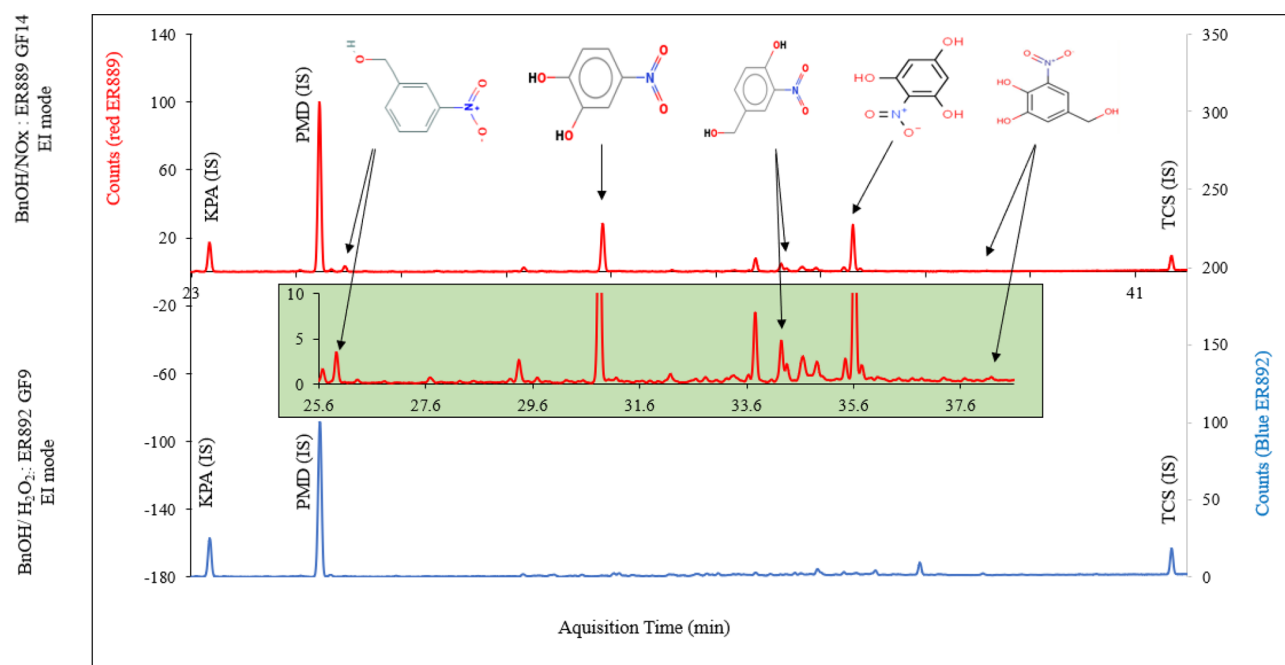
Figure 7. Portion of GC-MS extracted ion chromatograms (EI mode) at m/z 210, 165 (IS), 299 (IS), 300, 298, 372, and 388 associated with nitro-aromatic compounds merged in one chromatogram: (red) BnOH in the presence of NO_x (ER889); (blue) BnOH in the presence of H_2O_2 and absence of NO_x (ER892).

able based on the theoretical study of Wang (2015). Scheme 1 shows mechanistic pathways leading to the formation of stable products (blue) including BnAld, 4-hydroxybenzyl alcohol, 2-hydroxybenzyl alcohol, phenol, formaldehyde, and catechol. The initial branching ratios shown in Scheme 1 are those reported by Wang (2015), obtained by combining quantum chemistry calculations and experimental work from the literature. BnAld was observed in this study in the presence and absence of NO_x, and its secondary chemistry may in part lead to oxygenated compounds observed in this study (Bernard et al., 2013). Due to the large number of possible intermediates formed (Wang, 2015), only selected pathways energetically favorable, leading to some products observed in this study, are considered. We refer the readers to Wang (2015) for an in-depth theoretical analysis of mechanistic pathways leading to the formation of selected reaction products. The adduct R1 reacts rapidly through addition of O_2 to the ortho (C2) to produce peroxy radicals R1-2OO. The O_2 addition to the para position (C4) leading to R1-4OO peroxy radicals (not shown in Scheme 1) was found to be endothermic and therefore negligible (Wang, 2015). Radicals R1-2OO undergo intramolecular H shifts or ring closures to form a stable bicyclic intermediate R1-26OO (red). Similarly, R2 reacts rapidly with O_2 to form the peroxy radical R2-1OO intermediate, which itself undergoes intramolecular H shifts or ring closures to form a stable bicyclic intermediate R2-13OO (red). R1-26OO and R2-13OO intermediates undergo further reactions leading to ring-opening products as

shown in Scheme 3. 2-Hydroxybenzyl alcohol was proposed by Wang (2015) to form through the reaction of R2 with O_2 involving rapid direct H abstraction. A possible formation pathway of phenol is decomposition of the peroxy radicals R1-2OO and R2-1OO through CH_2OH radical elimination (Bernard et al., 2013). As in Wang (2015), the reverse reaction that gives R1 + O_2 is certainly competitive with the cyclization. Moreover, this reversible reaction sustains the concentration of R1 with the radical now delocalized within the aromatic structure rather than associated with the substituent O_2. By this approach, reactions of R1 lead to the formation of phenol and subsequent formation of catechol as shown in Scheme 1. However, we do not have quantitative product data that would give insight to the R1-2OO and R2-1OO decomposition (reverse) rate with respect to the O_2 cyclization rate. Note that the R1 reaction to form phenol is independent of NO_2, whereas the reaction of R1 to form nitrobenzyl alcohol is dependent on NO_2.

The CH_2OH radical reacts rapidly with O_2 to produce formaldehyde. Catechol was proposed to originate from the reaction of OH radicals with phenol (Atkinson et al., 1992) and with 2-hydroxybenzyl alcohol (Bernard et al., 2013).

NACs observed in this study (Table 7) are expected to be formed through reaction of OH radicals with BnOH in the presence of NO_2. Scheme 2 briefly summarizes the main mechanistic pathways leading to BnOH NACs, which follow similar chemistry as those reported for toluene, benzene, and xylenes (Jenkin et al., 2003; Vidovic et al., 2018)

**Table 7.** NACs identified in benzyl alcohol photooxidation in the presence of NO_x.

Nomenclature	Chemical Formula Rt (min)	m/z BSTFA Derivative (CH₄-CI) (EI)	MW (MWbstfa)	Observed in GP; PP [GP/PP ratio]	Proposed Structure
3-nitrobenzyl alcohol[a]	$C_7H_7NO_3$ (25.93)	226, 210, 180, 136, 73 210, 180, 165, 194, 73	153 (225)	PP, GP [1.71]	
4-nitrocatechol[a]	$C_6H_5NO_4$ (30.86)	300, 284, 328, 254, 73 73, 284, 299, 269, 223	155 (299)	PP, GP [0.08]	
2-hydroxy-5-nitro benzyl alcohol[a] (4 isomers)	$C_7H_7NO_4$ (34.26)	314, 298, 268, 342, 73 298, 283, 191, 314, 73	169 (313)	PP, GP [0.08]	
2-nitro phloroglucinol[a] (4 isomers)[b]	$C_6H_5NO_5$ (35.62)	388, 372, 416, 428, 73 73, 372, 387, 284, 306	171 (387)	PP	
3,4-dihydroxy-5-nitrobenzyl alcohol (4 isomers)[c]	$C_7H_7NO_5$ (38.18)	388, 372, 416, 428, 73 73, 224, 3876, 401, 356	185 (401)	PP	

[a] identified using authentic standards. [b] Three additional peaks eluted at 33.76, 34.70, 34.76 min with similar mass spectra as those recorded for 2-nitrophloroglucinol standard were detetcted, and the structure given here is for 2-nitrophloroglucinol. [c] Three additional peaks eluted at 35.94, 36.60, 38.18 min with similar mass spectra were detetcted.

as summarized by Wang et al. (2019). The steps shown in Scheme 2 are multi-steps, and the reader should consult the reference papers above for more in-depth information. NACs are proposed to originate from secondary reactions of catechol, 1,3,5-trihydroxy benzene, and 4-hydroxybenzyl alcohol with OH radicals in the presence of NO_2 (Scheme 2). These intermediates are proposed to originate from R1, R2, and R3 adducts. Additional pathways could be initiated via less well understood aqueous-phase nitration (Kroflic et al., 2018). 4-Nitrocatechol is proposed to be initiated through the reaction of catechol with OH radicals in the presence of NO_x (Finewax et al., 2018). 4-Hydroxy-2-nitrobenzyl alcohol is proposed to likely originate from the alkyldihydroxy-para adduct formed from the OH addition to the para position (Scheme 2). 2-Nitrophloroglucinol and 3,4-dihydroxy-5-nitrobenzyl alcohol follow similar reactions involving R3 adduct, OH radicals, and NO_2.

According to the Wang (2015) calculation, at high NO_2 (100 ppbv) the reaction of R1 with NO_2 can compete to a minor degree with the reaction with O_2, and therefore R1 possibly forms minor amounts of nitrobenzyl alcohol. This is similar to that of other alkylbenzenes, such as toluene, al-

though at much higher NO_2 concentrations (Wang, 2015). According to the Wang calculation at 100 ppb NO_2, up to 30 % of the R1 radical can form nitrobenzyl alcohol (unspecified nitro location on the ring). When including the R2 radical, which forms negligible levels of nitrobenzyl alcohol, no more than 20 % (and likely much less under our conditions) of the initial ring-retaining radical would form nitrobenzyl alcohol. As noted in the caption to Table 1, the initial NO_x is 98 % NO, and thus there is an extremely low initial concentration of NO_2. As the extent of reaction increases, the NO_y concentration increases as do other more oxidized forms of NO_x. Thus, the addition of NO_2 ($\sim$ 100 ppb) to the carbon-centered radical on the ring is of the same order as that described by Wang (2015) as being of minor importance compared to O_2 addition. Thus, even though NO_y concentrations in these experiments are higher than ambient concentrations, we consider the findings and mechanisms of Wang (2015) to be relevant to this work. We only have an upper limit to the NO_2 concentration: that is, NO_y is determined from NO_x–NO, as measured by the oxides-of-nitrogen (NO_x) monitor. It is well known that the NO_x monitor in the NO_x–NO chan-
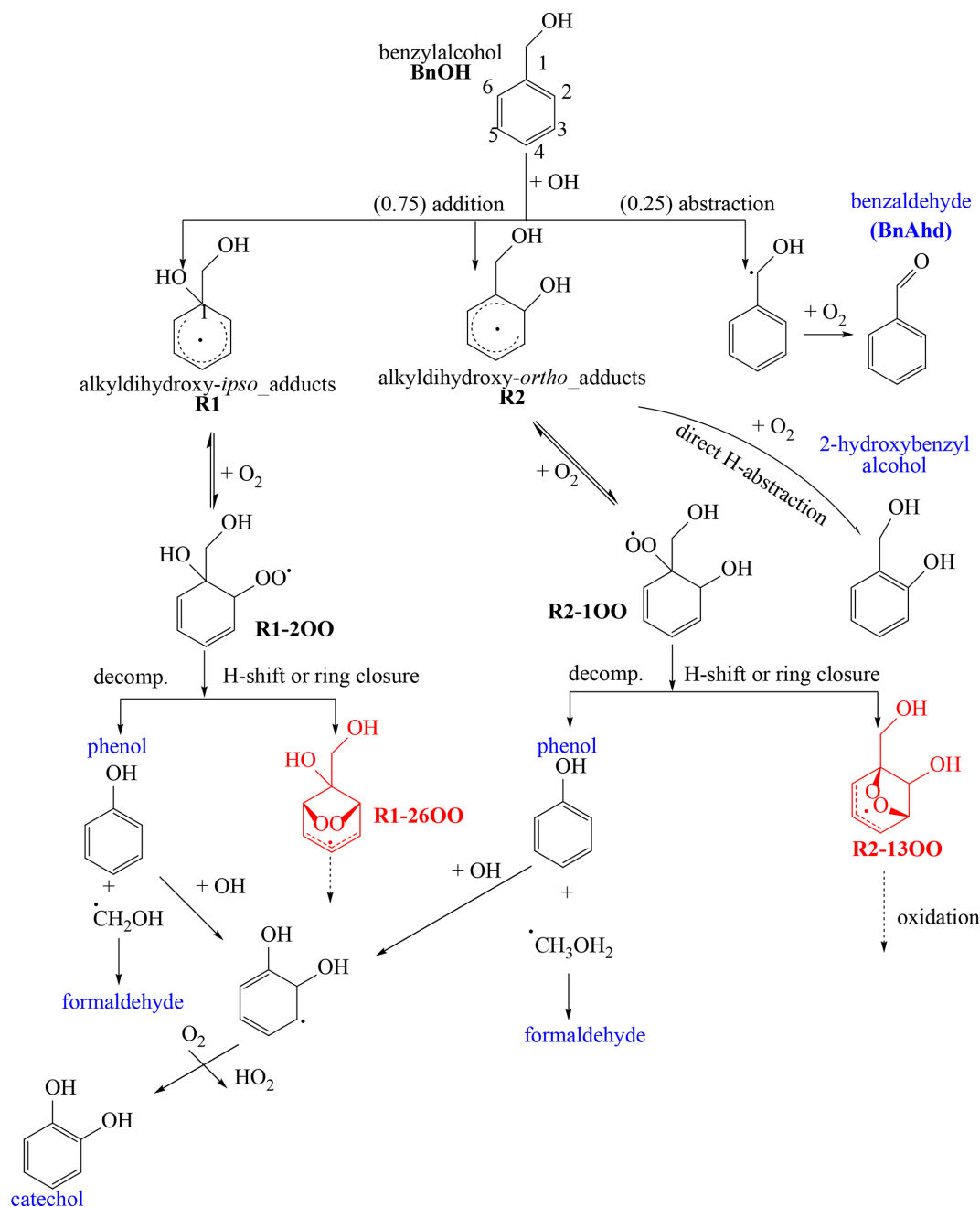
Scheme 1. Initial reaction pathways proposed to produce selected products detected in this study (blue) in the gas phase or PP (Table 5). R1-26OO and R2-13OO intermediates undergo further reactions leading to ring-opening products as shown in Scheme 3.

nel measures other oxidized organic compounds in addition to NO_2.

HOCs were detected in the PP from the oxidation of BnOH in both low- and high-NO_x systems (Table 6). Mechanistic pathways based on theoretical studies leading to several HOCs (e.g., HOMs) from the atmospheric oxidation of biogenic and aromatic hydrocarbons have been reported recently in the literature involving unimolecular reaction through autoxidation and peroxy and/or alkoxy radical isomerization

(Wang, 2015; Jaoui et al., 2021; Piletic and Kleindienst, 2022). The formation of selected HOCs observed in this study is consistent with the following pathways proposed in Scheme 3 involving the R2-1300 radical as the starting material. R1-26OO adduct undergoes similar reactions leading to butenedial and 2,3-epoxy-butanedial as shown in Scheme S1 in the Supplement. Tartaric acid, 2,3,5-trihydroxy-4-oxopentanoic acid, and pentaric acid, observed in this study for the first time, are proposed to be initiated by the oxida-
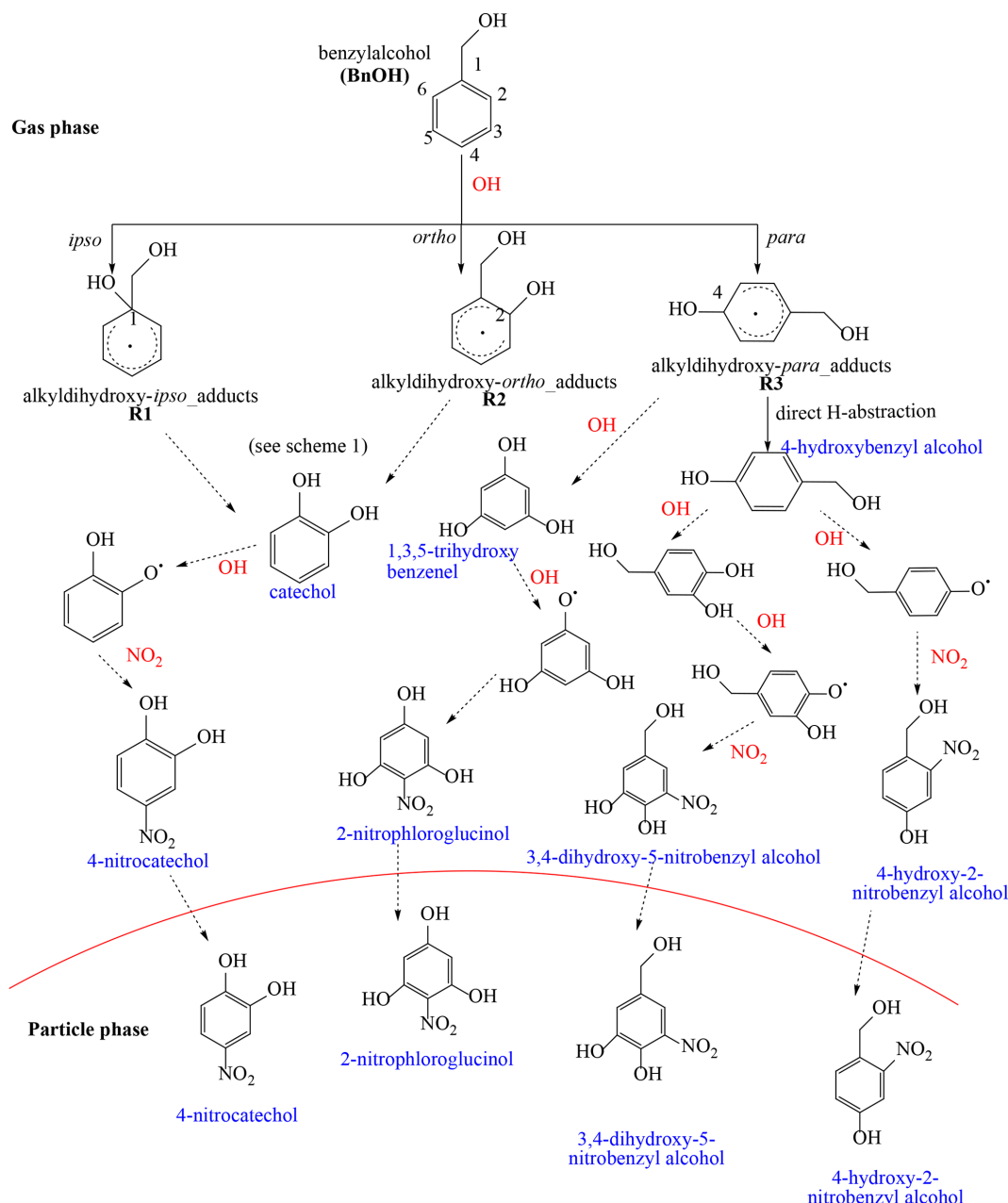
Scheme 2. Proposed mechanism for selected NAC species observed in this study.

tion of butenedial/2,3-epoxy-butanedial, 5-hydroxy-4-oxo-2-penatenal, and 4-hydroxy-2,3-epoxypentandial (Scheme 3). The mechanism leading to butenedial/2,3-epoxybutanal and 5-hydroxy-4-oxo-2-penatanal (Scheme S1) was reported by Wang (2015) from the OH oxidation of BnOH and is therefore not shown in Scheme 3. Tartaric acid present in the PP at a high level (Fig. 4) is proposed to be formed through the oxidation of butenedial and/or 2,3-epoxybutanal through classical oxidation of aldehydes and alkenes to carboxylic acid (not shown in Scheme 3). Similarly, 2,3,5-trihydroxy-4-oxo-pentanoic acid and pentaric acid are proposed to rise

from the oxidation of 5-hydroxy-4-oxo-2-pentenal and 4-hydroxy-2,3-epoxypentanedial, respectively, following similar mechanistic pathways reported by Jaoui et al. (2021) for the formation of methyltartaric acid from 4-hydroxy-2-methyl-but-2-enal involving peroxy and alkoxy radical isomerization (not reported here). In this study, a new mechanism is proposed in Scheme 3 leading to the formation of 4-hydroxy-2,3-epoxypentanedial, which is the starting material for pentaric acid formation. It involves several intermediate steps including unimolecular H migration (e.g., 1,5-H shift), ring opening, and decomposition. Formaldehyde and glyoxal
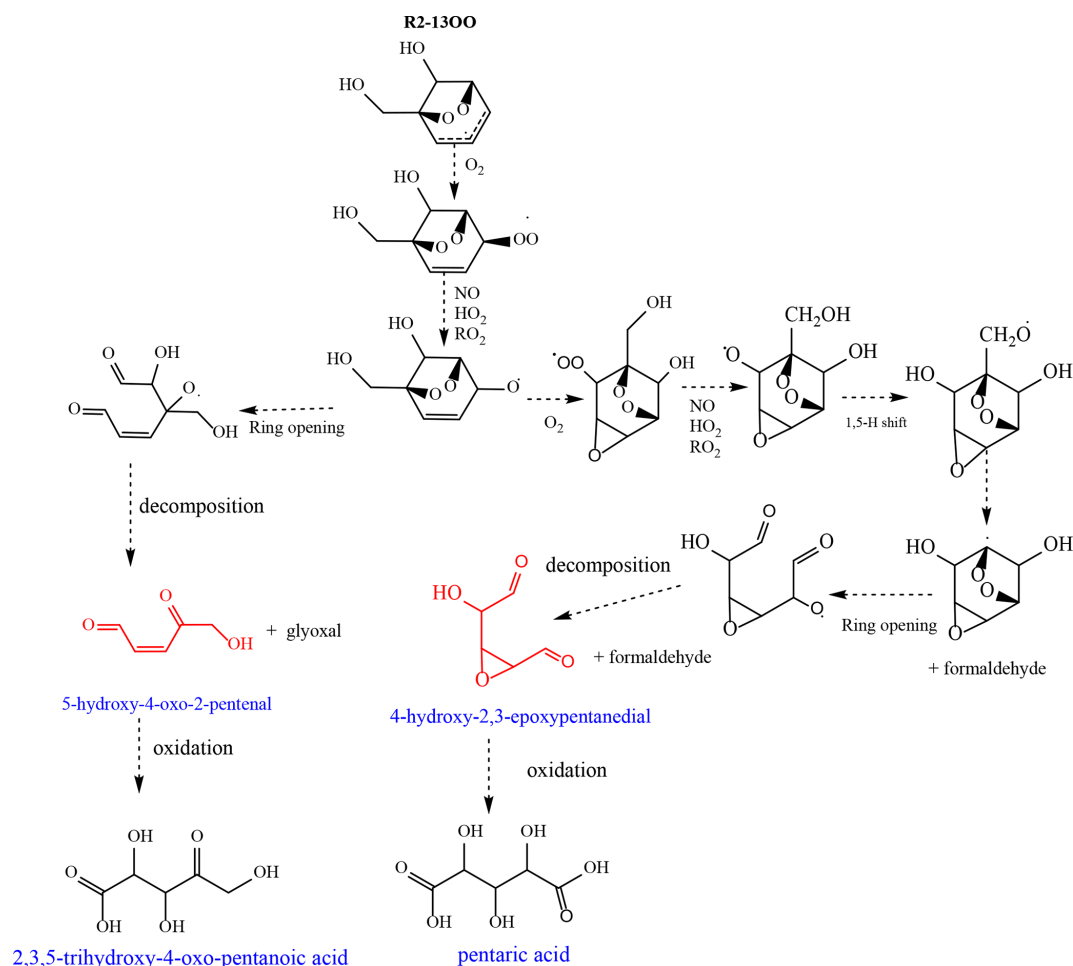
Scheme 3. Proposed mechanism for selected highly oxygenated compounds observed in this study.

observed in this study are also shown in Scheme 3. The data used to support the secondary reactions of R2-13OO are primarily product data shown in Scheme 3, which shows fragmentation products from R2-13OO. These products have been well known for alkylbenzenes for many years. We have used analogous pathways for these alkylbenzenes to provide an understanding as to how observed fragmentation products of BnOH are formed. However, it is important to note that these fragmentation pathways follow from the formation of alkoxy radicals and not peroxy radicals. Thus, NO is required in the system. (Note: $RO_2 + RO_2 \rightarrow 2RO + O_2$ is too slow to provide the alkoxy radicals needed for the fragmentation reaction to occur.) Similar pathways are also applicable for R1-26OO.

4 Summary

In the present paper, laboratory experiments were conducted to investigate SOA formation from the oxidation of benzyl alcohol in the presence and absence of NO_x. Chamber aerosol collected under these conditions has been analyzed for or-

ganic mass to organic carbon ratio and aerosol yield. In addition, the chemical composition of the gas phase and SOA was analyzed using derivative-based methods followed by gas chromatography–mass spectrometry and high-performance liquid chromatography analysis of the derivative compounds. More than 50 oxygenated organic compounds in the gas and particle phases were identified. While a detailed non-targeted analysis has been made, our primary focus has been to examine highly oxygenated and nitro-aromatic compounds. The major components include ring-opening products with a high oxygen-to-carbon ratio (e.g., malic acid, tartaric acid, arabic acid, 2,3,5-trihydroxy-4-oxo-pentanoic acid, and pentaric acid) and ring-retaining products (e.g., benzaldehyde, benzoic acid, catechol, 3-nitrobenzyl alcohol, 4-nitrocatechol, 2-hydroxy-5-nitrobenzyl alcohol, 2-nitrophloroglucidol, 5-(hydroxymethyl)-3-nitro-1,2-benzyl diol). The presence of some of these products in the gas and particle phases simultaneously provides evidence of their gas–particle partitioning. These oxygenated oxidation products made dominant contributions to the SOA particle composition in both low- and high-NO_x systems. Yields, organic mass to organic carbon

ratio, and proposed reaction schemes for selected compounds are provided.

Finally, a set of reaction pathways is proposed that accounts for selected reaction products observed in this study from BnOH photooxidation in the presence of OH radicals, including NACs and HOCs. The proposed mechanism is based on (1) theoretical studies previously reported in the literature and (2) mechanisms associated with oxidation of aromatics (e.g., benzene, toluene, xylenes). New pathways were proposed for the formation of newly observed highly oxygenated compounds tartaric acid, 2,3,5-trihydroxy-4-oxopentanoic acid, and pentaric acid. Butenedial/2,3epoxybutandial, 5-hydroxy-4-oxo-2-pentenal, and 4-hydroxy-2,3-expoxypentanedial were proposed as the starting intermediate species leading to these highly oxygenated compounds. While theoretical studies involving unimolecular reactions were developed focusing mainly on ring-containing products (Wang, 2015; Piletic and Kleindienst, 2022), similar theoretical investigations focusing on linear species (Jaoui et al., 2021) as HOCs reported in this study will help strengthen the pathways proposed here.

The results of this study potentially have atmospheric implications for areas impacted by benzyl alcohol, including urban and indoor areas, and contribute to understanding the formation of ambient SOA from oxygenated anthropogenic precursors. Nitro-aromatics are pollutants of concern due to their toxicity, light absorption properties, and relatively long residence times in the environment. HOCs may partition into pre-existing particles or be involved in new particle formation.

Author contributions. MJ: study conceptualization; standards and chamber sample analysis; data collection; result interpretation; writing original and revised drafts; communication. KSD: aerosol mass spectroscopy measurements and result interpretation. ML: conducted chamber experiments; data collection and analysis. TEK: supervision; study conceptualization; result interpretation; writing original and revised drafts.

References

Abend, A. M., Chung, L., Bibart, R. T., Brooks, M., and McCollum, D. G.: Concerning the stability of benzyl alcohol: formation of benzaldehyde dibenzyl acetal under aerobic conditions, J. Pharm. Biomed. Anal., 34, 957–962, https://doi.org/10.1016/j.jpba.2003.11.007, 2004.

Akherati, A., Cappa, C. D., Kleeman, M. J., Docherty, K. S., Jimenez, J. L., Griffith, S. M., Dusanter, S., Stevens, P. S., and Jathar, S. H.: Simulating secondary organic aerosol in a regional air quality model using the statistical oxidation model – Part 3: Assessing the influence of semi-volatile and intermediate-volatility organic compounds and NO_x, Atmos. Chem. Phys., 19, 4561–4594, https://doi.org/10.5194/acp-19-4561-2019, 2019.

Alton, M. W. and Browne, L. C.: Atmospheric chemistry of volatile methyl siloxanes: kinetics and products of oxidation by OH radicals and Cl atoms, Environ. Sci. Technol., 54, 5992–5999, 2020.

Antonelli, L., Mapelli, E., Strini, A., Cerulli, T., Leoni, R., and Stella S.: Laboratory and real scale comparative study of benzyl alcohol emission from a two-component epoxy paint, Proceedings: Proceedings, Indoor Air, 584–589, 2002.

Atkinson, R., Aschmann, S. M., and Arey, J.: Reactions of OH and N03 Radicals with Phenol, Cresols, and 2-Nitrophenol at 296 ± 2 K, Environ. Sci. Technol., 26, 1397–1403, 1992.

Bernard, B., Magneron, I., Eyglunent, G., Daële, V., Wallington, T. J., Hurley, M. D., and Mellouki, A.: Atmospheric chemistry of benzyl alcohol: kinetics and mechanism of reaction with OH radicals, Environ. Sci. Technol., 47, 3182–3189, 2013.

Berndt, T., Herrmann, H., Sipila, M., and Kulmala, M.: Highly oxidized second-generation products from the gas-phase reaction of OH radicals with isoprene, J. Phys. Chem. A, 120, 10150–10159, 2016.

Boatright, J., Negre, F., Chen, X., Kish, C. M., Wood, B., Peel, G., Orlova, I., Gang, D., Rhodes, D., and Dudareva, N.: Understand-

ing in vivo benzenoid metabolism in petunia petal tissue, Plant Physiol., 135, 1993–2011, 2004.

Carter, W. P. L., Malkina, I. L., Cocker III, D. R., and Song, C.: Environmental chamber studies of VOC species in architectural coating and mobile source emissions, South Coast Air Quality Management District Contract No. 03468, 2005.

Charan, S. M., Buenconsejo, R. S., and Seinfeld, J. H.: Secondary organic aerosol yields from the oxidation of benzyl alcohol, Atmos. Chem. Phys., 20, 13167–13190, https://doi.org/10.5194/acp-20-13167-2020, 2020.

Charan, S. M., Huang, Y., Buenconsejo, R. S., Li, Q., Cocker III, D. R., and Seinfeld, J. H.: Secondary organic aerosol formation from the oxidation of decamethylcyclopentasiloxane at atmospherically relevant OH concentrations, Atmos. Chem. Phys., 22, 917–928, https://doi.org/10.5194/acp-22-917-2022, 2022.

Cheng, C. T., Chan, M. N., and Wilson, K. R.: Importance of unimolecular HO_2 elimination in the heterogeneous OH reaction of highly oxygenated tartaric acid aerosol, J. Phys. Chem. A, 120, 5887–5896, https://doi.org/10.1021/acs.jpca.6b05289, 2016.

Coggon, M. M., Gkatzelis, G. I., McDonald, B. C., Gilman, J. B., Schwantes, R. H., Abuhassan, N., Aikin, K. C., Arendd, M. F., Berkoff, T. A., Brown, S. S., Campos, T. L., Dickerson, R. R., Gronoff, G., Hurley, J. F., Isaacman-VanWertz, G., Koss, A. R., Lia, M., McKeen, S. A., Mosharyd, F., Peischl, J., Pospisilova, V., Renh, X., Wilson, A., Wu, Y., Trainer, M., and Warneke, C.: Volatile chemical product emissions enhance ozone and modulate urban chemistry, P. Natl. Acad. Sci. USA, 118, e2026653118, https://doi.org/10.1073/pnas.2026653118, 2021.

DeBolt, S., Cook, D. R., and Ford, C. M.: L-Tartaric acid synthesis from vitamin C in higher plants, P. Natl. Acad. Sci. USA, 103, 5608–5613, https://doi.org/10.1073/pnas.0510864103, 2006.

Derrien, E., Ahmar, M., Martin-Sisteron, E., Raffin, G., Queneau, Y., Marion, P., Beyerle, M., Pinel, C., and Besson, M.: Oxidation of aldoses contained in softwood hemicellulose acid hydrolysates into aldaric acids under alkaline or noncontrolled pH conditions, Ind. Eng. Chem. Res., 57, 4543–4552, https://doi.org/10.1021/acs.iecr.8b00239, 2018.

Do, J. Y., Salunkhe, D. K., and Olson, L. E.: Isolation, identification and comparison of the volatiles of peach fruit as related to harvest maturity and artificial ripening, J. Food Sci., 34, 618–621, 1969.

Ferri, D., Mondelli, C., Krumeich, F., and Baiker, A.: Discrimination of active palladium sites in catalytic liquid-phase oxidation of benzyl alcohol, J. Phys. Chem. B., 110, 22982–22986, https://doi.org/10.1021/jp065779z, 2006.

Finewax, Z., de Gow, J. A., and Ziemann, P. J.: Identification and Quantification of 4-Nitrocatechol Formed from OH and NO_3 Radical-Initiated Reactions of Catechol in Air in the Presence of NO_x: Implications for Secondary Organic Aerosol Formation from Biomass Burning, Environ. Sci. Technol., 52, 1981–1989, https://doi.org/10.1021/acs.est.7b05864, 2018.

Fu, Zi., Xie, H., Elm, J., Guo, X., Fu, Zh., and Chen, J.: Formation of low-volatile products and unexpected high formaldehyde yield from the atmospheric oxidation of methylsiloxanes, Environ. Sci. Technol., 54, 7136–7145, https://doi.org/10.1021/acs.est.0c01090, 2020.

Gkatzelis, G. I., Coggon, M. M., McDonald, B. C., Peischl, J., Aikin, K. C., Gilman, J. B., Trainer, M., and Warneke, C.: Identifying volatile chemical product tracer com-

pounds in U.S. Cities, Environ. Sci. Technol., 55, 188–199, https://doi.org/10.1021/acs.est.0c05467, 2021.

Gowda, D., Kawamura, K., and Tachibana, E.: Identification of hydroxy- and keto-dicarboxylic acids in remote marine aerosols using gas chromatography/quadruple and time-of-flight mass spectrometry, Rapid Commun. Mass Spectrom., 30, 992–1000, https://doi.org/10.1002/rcm.7527, 2016.

Harrison, J. C. and Wells, J. R.: Gas-phase chemistry of benzyl alcohol: reaction rate constants and products with OH radical and ozone, Atmos. Environ., 43, 798–804, 2009.

Harrison, J. C. and Wells, J. R.: 2-Butoxyethanol and benzyl alcohol reactions with the nitrate radical: rate coefficients and gas-phase products, Int. J. Chem. Kinet., 44, 778–788, 2012.

Hayes, P. L., Carlton, A. G., Baker, K. R., Ahmadov, R., Washenfelder, R. A., Alvarez, S., Rappenglück, B., Gilman, J. B., Kuster, W. C., de Gouw, J. A., Zotter, P., Prévôt, A. S. H., Szidat, S., Kleindienst, T. E., Offenberg, J. H., Ma, P. K., and Jimenez, J. L.: Modeling the formation and aging of secondary organic aerosols in Los Angeles during CalNex 2010, Atmos. Chem. Phys., 15, 5773–5801, https://doi.org/10.5194/acp-15-5773-2015, 2015.

Hinton, M. R.: Xylaric acid, D-arabinaric acid (D-lyxaric acid), L-arabinaric acid (L-lyxaric acid), and Ribaric acid-1,4-lactone; Synthesis and isolation-synthesis of polyhydroxypolyamides therefrom, Theses, Dissertations, & Professional Papers, 1202, https://scholarworks.umt.edu/etd/1202 (last access: 14 September 2022), 2008.

Hodzic, A., Jimenez, J. L., Madronich, S., Aiken, A. C., Bessagnet, B., Curci, G., Fast, J., Lamarque, J.-F., Onasch, T. B., Roux, G., Schauer, J. J., Stone, E. A., and Ulbrich, I. M.: Modeling organic aerosols during MILAGRO: importance of biogenic secondary organic aerosols, Atmos. Chem. Phys., 9, 6949–6981, https://doi.org/10.5194/acp-9-6949-2009, 2009.

Horvat, R. J., Chapman Jr., G. W., Robertson, J. A., Meredith, F. I., Scorza, R., Callahan, A. M., and Morgens, P.: Comparison of the volatile compounds from several commercial peach cultivars, J. Agric. Food Chem., 38, 234–237, 1990.

Humes, M. B., Wang, M., Kim, S., Machesky, J. E., Gentner, D. R., Robinson, A. L., Donahue, N. M., and Presto, A. A.: Limited secondary organic aerosol production from acyclic oxygenated volatile chemical products, Environ. Sci. Technol., 56, 4806–4815, 2022.

Humpf, H. U. and Schreier, P.: Bound aroma compounds from the fruit and the leaves of blackberry (*Rubus laciniata* L.), J. Agric. Food Chem., 39, 1830–1832, 1991.

Ikemori, E., Nakayama, T., and Hasegawa, H.: Characterization and possible sources of nitrated mono- and di-aromatic hydrocarbons containing hydroxyl and/or carboxyl functional groups in ambient particles in Nagoya, Japan, Atmos. Environ., 211, 91–102, 2019.

Janechek, N. J., Marek, R. F., Bryngelson, N., Singh, A., Bullard, R. L., Brune, W. H., and Stanier, C. O.: Physical properties of secondary photochemical aerosol from OH oxidation of a cyclic siloxane, Atmos. Chem. Phys., 19, 1649–1664, https://doi.org/10.5194/acp-19-1649-2019, 2019.

Jaoui, M.: The Home of the U.S. Government's Open Data, U. S. Environmental Protection Agency, https://data.gov/ (last access: 14 September 2022), 2023.

Jaoui, M. and Kamens, R. M.: Mass balance of gaseous and particulate products analysis from α-pinene/NO_x/air in the pres-

ence of natural sunlight, J. Geophys. Res., 106, 12541–12558, https://doi.org/10.1029/2001JD900005, 2001.

Jaoui, M., Kleindienst, T. E., Lewandowski, M., and Edney, E. O.: Identification and quantification of aerosol polar oxygenated compounds bearing carboxylic and/or hydroxyl groups, 1. Method development, Anal. Chem., 76, 4765–4778, 2004.

Jaoui, M., Kleindienst, T. E., Lewandowski, M., Offenberg, J. H., and Edney, E. O.: Identification and quantification of aerosol polar oxygenated compounds bearing carboxylic or hydroxyl groups. 2. Organic tracer compounds from monoterpenes, Environ. Sci. Technol., 39, 5661–5673, 2005.

Jaoui, M., Kleindienst, T. E., Docherty, K. S., Lewandowski, M., and Offenberg, J. H.: Secondary organic aerosol formation from the oxidation of a series of sesquiterpenes: a-cedrene, b-caryophyllene, a-humulene and a-farnesene with O$_3$, OH and NO$_3$ radicals, Environ. Chem., 10, 178–193, https://doi.org/10.1071/EN13025, 2013.

Jaoui, M., Lewandowski, M., Docherty, K., Offenberg, J. H., and Kleindienst, T. E.: Atmospheric oxidation of 1,3-butadiene: characterization of gas and aerosol reaction products and implications for PM$_{2.5}$, Atmos. Chem. Phys., 14, 13681–13704, https://doi.org/10.5194/acp-14-13681-2014, 2014.

Jaoui, M., Lewandowski, M., Offenberg, H. J., Colon, M., Docherty, K. S., and Kleindienst, T. E: Characterization of aerosol nitroaromatic compounds: Validation of an experimental method, Mass Spectrom., 53, 680–692, 2018.

Jaoui, M., Szmigielski, R., Nestorowicz, K., Kolodziejczyk, A., Sarang, K., Rudzinski, K. J., Konopka, A., Bulska, E, Lewandowski, M., and Kleindienst, T. E.: Organic hydroxy acids as highly oxygenated molecular (HOM) tracers for aged isoprene aerosol, Environ. Sci. Technol., 53, 14516–14527, https://doi.org/10.1021/acs.est.9b05075, 2019.

Jaoui, M., Piletic, I., Szmigielski, R., Rudzinski, J. K., E, Lewandowski, M., Riedel, T. P., and Kleindienst, T. E.: Rapid production of highly oxidized molecules in isoprene aerosol via peroxy and alkoxy radical isomerization pathways in low and high NO$_x$ environments: Combined laboratory, computational and field studies, Sci. Total Environ., 775, 145592, https://doi.org/10.1016/j.scitotenv.2021.145592, 2021.

Jenkin, M. E., Saunders, S. M., Wagner, V., and Pilling, M. J.: Protocol for the development of the Master Chemical Mechanism, MCM v3 (Part B): tropospheric degradation of aromatic volatile organic compounds, Atmos. Chem. Phys., 3, 181–193, https://doi.org/10.5194/acp-3-181-2003, 2003.

Khare, P. and Gentner, D. R.: Considering the future of anthropogenic gas-phase organic compound emissions and the increasing influence of non-combustion sources on urban air quality, Atmos. Chem. Phys., 18, 5391–5413, https://doi.org/10.5194/acp-18-5391-2018, 2018.

Kleindienst, T. E., Edney, E. O., Lewandowski, M., Offenberg, J. H., and Jaoui M.: Secondary organic carbon and aerosol yields from the irradiations of isoprene and α-pinene in the presence of NO$_x$ and SO$_2$, Environ. Sci. Technol., 40, 3807–3812, 2006.

Kleindienst, T. E., Lewandowski, M., Offenberg, J. H., Jaoui, M., and Edney, E. O.: The formation of secondary organic aerosol from the isoprene + OH reaction in the absence of NO$_x$, Atmos. Chem. Phys., 9, 6541–6558, https://doi.org/10.5194/acp-9-6541-2009, 2009.

Kleindienst, T. E., Jaoui, M., Lewandowski, M., Offenberg, J. H., and Docherty, K. S.: The formation of SOA and chemical tracer compounds from the photooxidation of naphthalene and its methyl analogs in the presence and absence of nitrogen oxides, Atmos. Chem. Phys., 12, 8711–8726, https://doi.org/10.5194/acp-12-8711-2012, 2012.

Kroflic, A., Hus, M., Grilc, M., and Grgic, I.: Underappreciated and complex role of nitrous acid in aromatic nitration under mild environmental conditions: the case of activated methoxyphenols, Environ. Sci. Technol., 52, 13756–13765, https://doi.org/10.1021/acs.est.8b01903, 2018.

Kroll, J. H., Chan, A. W. H., Ng, N. L., Flagan, R. C., and Seinfeld, J. H.: Reactions of semivolatile organics and their effects on secondary organic aerosol formation, Environ. Sci. Technol., 41, 3545–3550, 2007.

Larsen, M. and Poll, L.: Odor thresholds of some important aroma compounds in raspberries, Z. Lebensm. Unters. Forsch, 191, 129–131, 1990.

Lewandowski, M., Jaoui, M., Offenberg, J. H., Krug, J. D., and Kleindienst, T. E.: Atmospheric oxidation of isoprene and 1,3-butadiene: influence of aerosol acidity and relative humidity on secondary organic aerosol, Atmos. Chem. Phys., 15, 3773–3783, https://doi.org/10.5194/acp-15-3773-2015, 2015.

Li, W., Li, L., Chen, C-L, Kacarab, M., Peng, W., Price, D., Xu, J., and Cocker III, D. R.: Potential of select intermediate-volatility organic compounds and consumer products for secondary organic aerosol and ozone formation under relevant urban conditions, Atmos. Environ., 118, 109–117, 2018.

Lu, Q., Murphy, B. N., Qin, M., Adams, P. J., Zhao, Y., Pye, H. O. T., Efstathiou, C., Allen, C., and Robinson, A. L.: Simulation of organic aerosol formation during the CalNex study: updated mobile emissions and secondary organic aerosol parameterization for intermediate-volatility organic compounds, Atmos. Chem. Phys., 20, 4313–4332, https://doi.org/10.5194/acp-20-4313-2020, 2020.

McDonald, B. C., De Gouw, J. A., Gilman, J. B., Jathar, S. H., Akherati, A., Cappa, C. D., Jimenez, J. L., Lee-Taylor, J., Hayes, P. L., McKeen, S. A., Cui, Y. Y., Kim, S. W., Gentner, D. R., Isaacman-VanWertz, G., Goldstein, A. H., Harley, R. A., Frost, G. J., Roberts, J. M., Ryerson, T. B., and Trainer, M.: Volatile chemical products emerging as largest petrochemical source of urban organic emissions, Science, 359, 760–764, 2018.

Milani, A., Al-Naiema, I. M., and Stone, E. A: Detection of a secondary organic aerosol tracer derived from personal care products, Atmos. Environ., 246, 118078, https://doi.org/10.1016/j.atmosenv.2020.118078, 2021.

Mohr, C., DeCarlo, P. F., Heringa, M. F., Chirico, R., Richter, R., Crippa, M., Querol, X., Baltensperger, U., and Prévôt, A. S. H.: Spatial variation of aerosol chemical composition and organic components identified by positive matrix factorization in the Barcelona region, Environ. Sci. Technol., 49, 10421–10430, 2015.

Namysl, S., Pelucchi, M., Maffei, L. P., Herbinet, O., Stagni, A., Faravelli, T., and Battin-Leclerc, F.: Experimental and modeling study of benzaldehyde oxidation, Combustion and Flame, 211, 124–132, 2020.

Offenberg, J. H., Lewandowski, M., Edney, E. O., Kleindienst, T. E., and Jaoui, M.: Investigation of a systematic offset in the measurement of organic carbon with a semicontinuous an-

alyzer, J. A&WMA, 57, 596–599, https://doi.org/10.3155/1047-3289.57.5.596, 2007.

Orlova, I., Marshall-Colòn, A., Schnepp, J., Wood, B., Varbanova, M., Fridman, E., Blakeslee, J. J., Peer, W. A., Murphy, A. S., Rhodes, D., Pichersky, E., and Dudareva, N.: Reduction of Benzenoid synthesis in petunia flowers reveals multiple pathways to benzoic acid and enhancement in auxin transport, Plant Cell, 18, 3458–3475, 2006.

Pennington, E. A., Seltzer, K. M., Murphy, B. N., Qin, M., Seinfeld, J. H., and Pye, H. O. T.: Modeling secondary organic aerosol formation from volatile chemical products, Atmos. Chem. Phys., 21, 18247–18261, https://doi.org/10.5194/acp-21-18247-2021, 2021.

Piletic, I. R. and Kleindienst, T. E.: Rates and Yields of Unimolecular Reactions Producing Highly Oxidized Peroxy Radicals in the OH-Induced Autoxidation of α-Pinene, β-Pinene, and Limonene, J. Phys. Chem. A, 126, 88–100, https://doi.org/10.1021/acs.jpca.1c07961, 2022.

Qin, M. M., Murphy, B. N., Isaacs, K. K., McDonald, B. C., Lu, Q. Y., McKeen, S. A., Koval, L., Robinson, A. L., Efstathiou, C., Allen, C., and Pye, H. O. T.: Criteria pollutant impacts of volatile chemical products informed by near-field modelling, Nature Sustainability, 4, 129–137, https://doi.org/10.1038/s41893-020-00614-1, 2021.

Röhrl, A. and Lammel, G.: Determination of malic acid and other C4 dicarboxylic acids in atmospheric aerosol samples, Chemosphere, 46, 1195–1199, https://doi.org/10.1016/s0045-6535(01)00243-0, 2002.

Sankar, S., Nowicka, E., Carter, E., Murphy, D. M., Knight, D. W., Bethell, D., and Hutchings, G. J.: The benzaldehyde oxidation paradox explained by the interception of peroxy radical by benzyl alcohol, Nat. Commun., 5, 3332, https://doi.org/10.1038/ncomms4332, 2014.

Seltzer, K. M., Murphy, B. N., Pennington, E. A., Allen, C., Talgo, K., and Pye, H. O. T.: Volatile chemical product enhancements to criteria pollutants in the United States, Environ. Sci. Technol., 56, 6905–6913, https://doi.org/10.1021/acs.est.1c04298, 2021.

Shilling, J. E., Chen, Q., King, S. M., Rosenoern, T., Kroll, J. H., Worsnop, D. R., McKinney, K. A., and Martin, S. T.: Particle mass yield in secondary organic aerosol formed by the dark ozonolysis of α-pinene, Atmos. Chem. Phys., 8, 2073–2088, https://doi.org/10.5194/acp-8-2073-2008, 2008.

Smith, D. F., Kleindienst, T. E., and Hudgens, E. E.: Improved high-performance liquid chromatographic method for artifact free measurements of aldehydes in the presence of ozone using 2,4-dinitrophenylhydrazine, J. Chromatogr. A, 483, 431–436, 1989.

Stockwell, C. E., Coggon, M. M., Gkatzelis, G. I., Ortega, J., McDonald, B. C., Peischl, J., Aikin, K., Gilman, J. B., Trainer, M., and Warneke, C.: Volatile organic compound emissions from solvent- and water-borne coatings – compositional differences and tracer compound identifications, Atmos. Chem. Phys., 21, 6005–6022, https://doi.org/10.5194/acp-21-6005-2021, 2021.

Urakami, K., Kobayashi, C., Miyazaki, Y., Nishijima, K., and Yoshimura, Y.: Degradation products generated by sonication of benzyl alcohol, a sample preparation solvent for the determination of residual solvents in pharmaceutical bulks, on capillary gas chromatography, Chem. Pharm. Bull., 48, 1299–1303, 2000.

Vallat, A. and Dorn, S.: Changes in volatile emissions from apple trees and associated response of adult female codling moths over the fruit-growing season, J. Agric. Food Chem., 53, 4083–4090, 2005.

Vidovic, K., Lasic Jurkovic, D., Sala, M., Kroflic, A., and Grgic, I.: Nighttime aqueous-phase formation of nitrocatechols in the atmospheric condensed phase, Environ. Sci. Technol., 52, 9722–9730, https://doi.org/10.1021/acs.est.8b01161, 2018.

Vlachou, A., Daellenbach, K. R., Bozzetti, C., Chazeau, B., Salazar, G. A., Szidat, S., Jaffrezo, J.-L., Hueglin, C., Baltensperger, U., Haddad, I. E., and Prévôt, A. S. H.: Advanced source apportionment of carbonaceous aerosols by coupling offline AMS and radiocarbon size-segregated measurements over a nearly 2-year period, Atmos. Chem. Phys., 18, 6187–6206, https://doi.org/10.5194/acp-18-6187-2018, 2018.

Wang, L.: The atmospheric oxidation mechanism of benzyl alcohol initiated by OH radicals: the addition channels, Chem. Phys. Chem., 16, 1542–1550, https://doi.org/10.1002/cphc.201500012, 2015.

Wang, N., Jorga, S. D., Pierce, J. R., Donahue, N. M., and Pandis, S. N.: Particle wall-loss correction methods in smog chamber experiments, Atmos. Meas. Tech., 11, 6577–6588, https://doi.org/10.5194/amt-11-6577-2018, 2018.

Wang, Y., Hu, M., Wang, Y., Zheng, J., Shang, D., Yang, Y., Liu, Y., Li, X., Tang, R., Zhu, W., Du, Z., Wu, Y., Guo, S., Wu, Z., Lou, S., Hallquist, M., and Yu, J. Z.: The formation of nitro-aromatic compounds under high NO_x and anthropogenic VOC conditions in urban Beijing, China, Atmos. Chem. Phys., 19, 7649–7665, https://doi.org/10.5194/acp-19-7649-2019, 2019.

Weschler, C. J.: Chemistry in indoor environments: 20 years of research, Indoor Air, 21, 205–218, 2011.

Wu, Y. and Johnston, M. V.: Molecular characterization of secondary aerosol from oxidation of cyclic methylsiloxanes, J. Am. Soc. Mass. Spectr., 27, 402–409, https://doi.org/10.1007/s13361-015-1300-1, 2016.

Wu, Y. and Johnston, M. V.: Aerosol formation from OH oxidation of the volatile cyclic methyl siloxane (cVMS) Decamethylcyclopentasiloxane, Environ. Sci. Technol., 51, 4445–4451, https://doi.org/10.1021/acs.est.7b00655, 2017.

Zhang, X., Cappa, C. D., Jathar, S. H., McVay, R. C., Ensberg, J. J., Kleeman, M. J., and Seinfeld, J. H.: Influence of vapor wall loss in laboratory chambers on yields of secondary organic aerosol, P. Natl. Acad. Sci. USA, 111, 5802–5807, https://doi.org/10.1073/pnas.1404727111, 2014.

Zhao, B., Wang, S., Donahue, N. M., Jathar, S. H., Huang, X., Wu, W., Hao, J., and Robinson, A. L.: Quantifying the effect of organic aerosol aging and intermediate volatility emissions on regional-scale aerosol pollution in China, Sci. Rep., 6, 28815, https://doi.org/10.1038/srep28815, 2016.